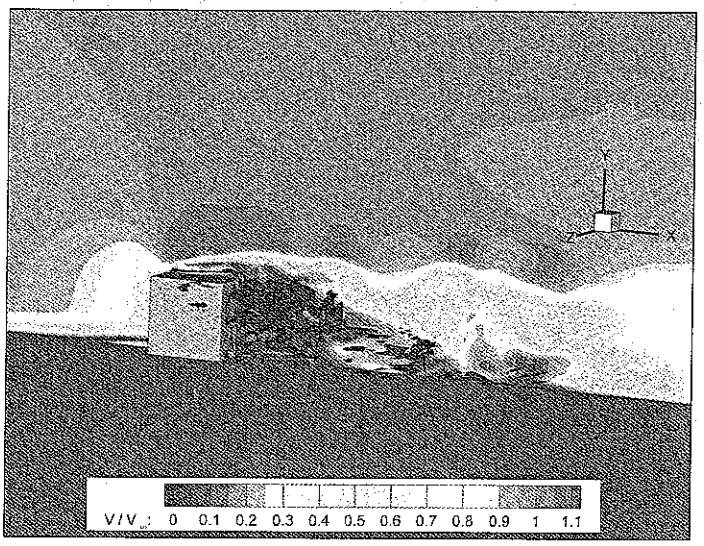

Introduction to **Chemical Transport in the Environment**

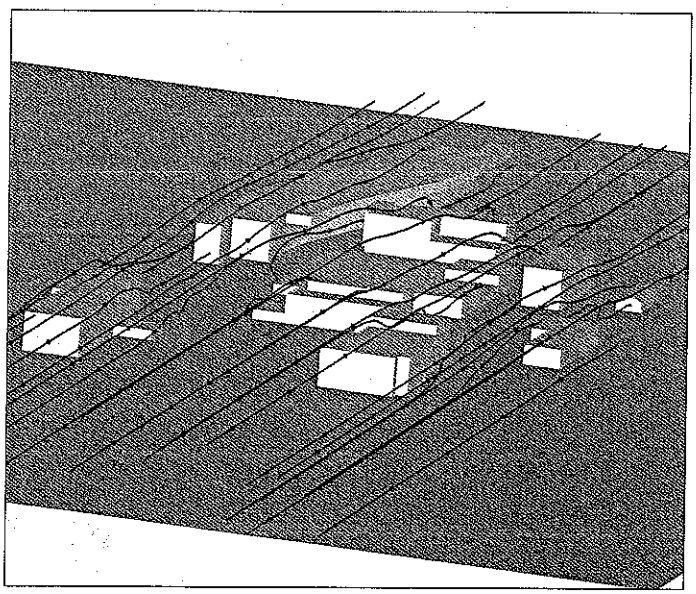

John S. Gulliver

CAMBRIDGE

Estimating the transport and fate of chemicals released into the environment is an interesting and challenging task. The global environment is large on the chemical transport and fate scale. This text applies the mathematics of diffusion, turbulent diffusion, and dispersion to the atmosphere, lakes, rivers, groundwater, and oceans, as well as transport between these media. The book follows a new educational paradigm of textbooks, in that it is based on examples and case studies. The required theory is explained as a technique for solving the case studies and example problems. A large portion of the book is dedicated to examples and case studies, from which the important principles are derived.

Dr. John S. Gulliver is the Joseph T. and Rose S. Ling Professor of Civil Engineering in the Department of Civil Engineering at the University of Minnesota, with an educational background in chemical engineering and civil engineering. His major engineering interests are in environmental fluid mechanics, chemical transport in environmental systems, and flow and chemical transport at hydraulic structures, on which he has published 98 peer-reviewed articles. He has investigated the measurement and prediction of air–water mass transfer at hydraulic structures, in river systems, at aerating hydroturbines, and in sparged systems and membrane aeration in reservoirs. He has investigated turbulent mixing and dispersion in lakes, reservoirs, and rivers and the fate and transport of a spilled nonaqueous phase liquid. He has developed numerical models to predict chemical and thermal transport and fate in rivers, reservoirs, and lakes. Dr. Gulliver has also advised on the efforts to reduce dissolved nitrogen concentrations downstream of dam spillways, consulted on techniques to remediate low dissolved oxygen concentrations that can occur in hydroelectric releases, and worked on forensic analysis of water quality problems that occur during operation of power facilities. He is coeditor of the *Hydropower Engineering Handbook*, *Air–Water Mass Transfer: Selected Papers from the Second International Symposium on Gas Transfer at Water Surfaces*, and *Energy and Sustainable Development Sub-Theme D, Proceedings of the 27th Congress of the International Association for Hydraulic Research*. He is currently the Coordinator of the Hydropower Institute. Dr. Gulliver received the Rickey Medal in 2003 from the American Society of Civil Engineers. He has been a visiting professor at the University of Karlsruhe, the University of São Paulo–São Carlos, Louisiana State University, and the University of Chile, where he served as a Fulbright Scholar. He also served as a visiting research scientist at the Waterways Experiment Station of the U.S. Army Corps of Engineers.

Cover illustrations: Calculated velocity field for wind blowing around an isolated building (left) and streamlines for wind flow through a building complex (right). Both courtesy of ARL (Penn State) Computational Mechanics.

Cover design by Alice Soloway

CAMBRIDGE
UNIVERSITY PRESS
www.cambridge.org

ISBN 978-0-521-85850-2

near a boundary that is important to the interaction with the diffusive boundary layer.

The eddy diffusion coefficients that we introduced in Chapter 5 were steady quantities, using mean turbulence quantities (e.g., the temporal mean of $u'C'$). This temporal mean character of eddy diffusion coefficients can be misleading in determining the thickness of a diffusive boundary layer because of the importance of unsteady characteristics. We will review some conceptual theories of mass transfer that have been put forward to describe the interaction of the diffusive boundary layer and turbulence.

1. Stagnant Film Theory

The stagnant film theory was developed by Nernst (1904). In this theory, a stagnant film exists on both sides of the interface, as illustrated in Figure 8.8. The thickness of the film is controlled by turbulence and is constant.

With the steady-state situation seen in Figure 8.8, $\partial C/\partial t \Rightarrow 0$, $\partial C/\partial x$ and $\partial C/\partial y \Rightarrow 0$, and $w \Rightarrow 0$. Then, the diffusion equation in each media, as long as turbulence does not penetrate the concentration boundary layer, becomes

$$D_a \frac{\partial^2 C_a}{\partial z^2} = 0 \qquad D_w \frac{\partial^2 C_w}{\partial z^2} = 0 \tag{8.22}$$

that results in a constant gradient of concentration:

$$\frac{\partial C_a}{\partial z} = \text{const.} \qquad \frac{\partial C_w}{\partial z} = \text{const.} \tag{8.23}$$

Now, at the interface, the flux in the air phase must equal the flux in the water phase:

$$J_a = -D_a \frac{\partial C_a}{\partial z} \qquad J_w = -D_w \frac{\partial C_w}{\partial z} \tag{8.24}$$

In addition, we can also apply these equations at the interface:

$$J_a = -k_G\left(C_a^{\infty} - C_a^i\right) \qquad J_w = -k_L\left(C_w^{\infty} - C_w^i\right) \tag{8.25}$$

where C^{∞} is the concentration away from the interface and C^i is the concentration at the interface. Because $\partial C/\partial z$ is constant,

$$\frac{\partial C_a}{\partial z} = \frac{C_a^{\infty} - C_a^i}{\delta_a} \qquad \frac{\partial C_w}{\partial z} = \frac{C_w^{\infty} - C_{wa}^i}{\delta_w} \tag{8.26}$$

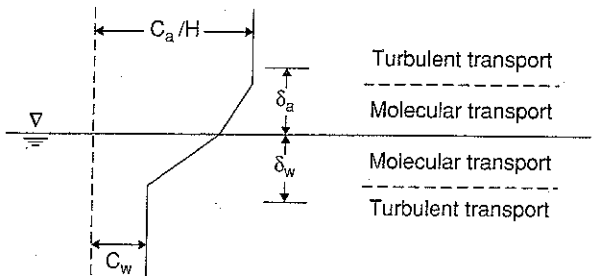

Figure 8.8. Concentration gradient at the interface as assumed by the stagnant film theory.

If we combine equations (8.24) to (8.26), we get

$$K_G = \frac{D_a}{\delta_a} \qquad K_L = \frac{D_w}{\delta_w} \tag{8.27}$$

or

$$Sh_a = \frac{K_G \delta_a}{D_a} = 1 \qquad Sh_w = \frac{K_L \delta_w}{D_w} = 1 \tag{8.28}$$

where Sh is a Sherwood number. Equations (8.27) and (8.28), however, are often valid with one caveat: δ_a and δ_w are not constant, but are a function of time and the diffusion coefficient.

2. Penetration Theory

The penetration theory is attributed to Higbie (1935). In this theory, the fluid in the diffusive boundary layer is periodically removed by eddies. The penetration theory also assumes that the viscous sublayer, for transport of momentum, is thick, relative to the concentration boundary layer, and that each renewal event is complete or extends right down to the interface. The diffusion process is then continually unsteady because of this periodic renewal. This process can be described by a generalization of equation (E8.5.6):

$$\frac{C - C^\infty}{C^i - C^\infty} = \text{erfc}\left(\frac{z}{\sqrt{4Dt}}\right) \tag{8.29}$$

Because the interfacial flux is given as

$$J = -D\frac{\partial C}{\partial z} \tag{8.30}$$

Equations (8.29) and (8.30) result in

$$J = \sqrt{\frac{D}{\pi t}}\, e^{-z^2/4Dt}(C^i - C^\infty) \tag{8.31}$$

or, at $z = 0$,

$$J\,|_{z=0} = \sqrt{\frac{D}{\pi t}}(C^i - C^\infty) \tag{8.32}$$

Combining equation (8.32) with (8.25) provides expressions for both K_L and K_G:

$$K_L = \sqrt{\frac{D_w}{\pi\, t_e}} \qquad K_G = \sqrt{\frac{D_a}{\pi\, t_e}} \tag{8.33}$$

Higbie hypothesized a constant time between events, labeled t_e. After each renewal event, the process of diffusive boundary layer growth would start over again. The diffusive boundary layer growth at one location is illustrated in Figure 8.9. Note that K_L and K_G are now proportional to $(D/t_e)^{1/2}$, instead of D/δ.

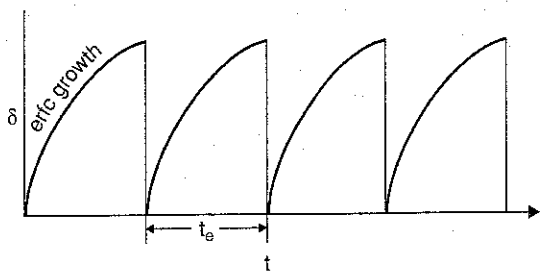

Figure 8.9. Concentration boundary layer growth as visualized by Higbie's penetration theory.

3. Surface Renewal Theory

Developed by Danckwerts (1951), the surface renewal theory states that t_e is not constant, but the renewal of the interface by turbulent eddies will have a period that is represented by a Gaussian distribution with respect to time. Then, K_L or K_G are given by the equation

$$K_L = \sqrt{D_w r} \qquad K_G = \sqrt{D_a r} \tag{8.34}$$

where r is the mean renewal rate (s^{-1}). The assumed thickness of the concentration boundary layer is similar to that given in Figure 8.10.

Instead of determining t_e, in equation (8.33), we must determine r in equation (8.34). Although the difference between Higbie's penetration theory and Danckwerts' surface renewal theory is not great, the fact that a statistical renewal period would have a similar result to a fixed renewal period brought much credibility to Higbie's penetration theory. Equation (8.34) is probably the most used to date, where r is a quantity that must be determined from the analysis of experimental data.

Characterizing Mean Renewal Rate. The mean renewal rate, r, can be characterized using dimensional analysis. Because r has units of inverse time, the characterization

$$r = V^2/\nu \tag{8.35}$$

will result in the appropriate dimensions, where V is some velocity relevant to the problem and ν is kinematic viscosity. If we use the liquid film as an example, then equation (8.34) becomes

$$K_L = \alpha V \sqrt{\frac{D_w}{\nu_w}} \tag{8.36}$$

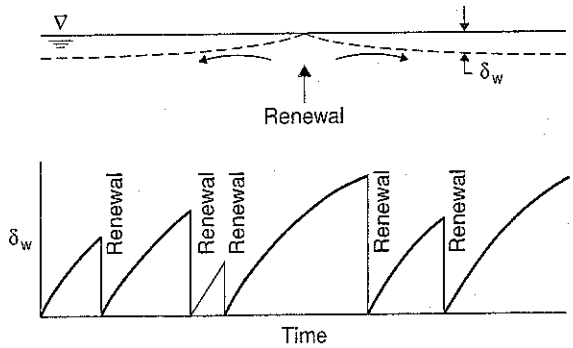

Figure 8.10. Conceptual sketches of surface renewal on the water side of the interface (top) and of the concentration boundary layer thickness at one location over time (bottom), as assumed by the surface renewal theory.

where α is a constant that depends on the application of equation (8.36). This equation may also be written as

$$St\, Sc^{1/2} = \alpha \tag{8.37}$$

or

$$\frac{Sh}{Re} Sc^{1/2} = \alpha \tag{8.38}$$

where St is a Stanton number (K_L/V), Sc is a Schmidt number (ν/D_w), Sh is a Sherwood number $(K_L L/D_w)$, and Re is a Reynolds number (VL/ν), and L is some length scale of the flow.

We can also replace V with a shear velocity, $u_* = (\tau/\rho)^{1/2}$, where τ is the interface shear stress and ρ is the density of the fluid. Again, equation (8.34) becomes

$$K_L = \alpha u_* \sqrt{\frac{D_w}{\nu_w}} \tag{8.39}$$

or

$$St^* = \alpha\, Sc^{1/2} \tag{8.40}$$

or

$$Sh = \alpha\, Sc^{1/2} Re^* \tag{8.41}$$

where St^* and Re^* use the shear velocity. Characteristic relations similar to equations (8.39) through (8.41) are commonly used in interfacial mass transfer, because shear velocity is a common representative of the turbulence, and the effect of the turbulence on the concentration boundary layer is what these equations are attempting to represent.

Careful experimentation and analysis by many independent investigators have shown us the following:

a. At fluid–fluid interfaces, $K_L \sim D_w^{1/2}$ and $K_G \sim D_a^{1/2}$ (Daniil and Gulliver, 1991; McCready et al., 1986). The surface renewal theory can be made to fit the transfer data at fluid–fluid interfaces. The exception to this is bubbles with a diameter less than approximately 0.5 mm. Even though there is a fluid on both sides, surface tension causes these small bubbles to behave as though they have a solid–fluid interface. There is also some debate about this 1/2 power relationship at free surfaces exposed to low shear, such as wind–wave flumes at low wind velocity (Jähne et al., 1987) and tanks with surfactants and low turbulence generation (Asher et al., 1996). The difficulty is that these results are influenced by the small facilities used to measure K_L, where surfactants will be more able to restrict free-surface turbulence and the impact on field scale gas transfer has not been demonstrated.
b. At solid–fluid interfaces, $K_L \sim D_w^{2/3}$ and $K_G \sim D_a^{2/3}$ (Campbell and Hanratty, 1982). These data cannot be made to fit the surface renewal theory because the theory gives $K_L \sim D_w^{1/2}$ and $K_G \sim D_a^{1/2}$.

4. Analogy to a Laminar Boundary Layer

Laminar boundary layer theory assumes that a uniform flow ($V = \text{constant}$) approaches a flat plate. A laminar flow region develops near the plate where the thickness of the laminar boundary layer increases with thickness along the plate, as developed in Example 4.2. If we assign δ to be the boundary layer thickness, or the distance from the plate where the velocity is equal to 0.99 times the velocity that approached the plate, and δ_c to be the concentration boundary layer thickness, then we can see that both δ and δ_c are functions of distance, x, from the leading edge, as shown in Figure 8.11.

Example 4.4 gave the following derivation for the boundary layer thickness:

$$\frac{\delta}{x} = 4.64\ Re_x^{-1/2} \tag{8.42}$$

where $Re_x = x\,V^\infty/\nu$ and V^∞ is the velocity approaching the plate. For a concentration boundary layer on a solid surface (Bird et al., 1960):

$$\frac{\delta_c}{x} = 4.64\ Re_x^{-1/2}\ Sc^{-1/3} \tag{8.43}$$

If we average the concentration flux over a given length, L, we get

$$Sh = 0.626\ Re_L^{1/2} Sc^{1/3} \tag{8.44}$$

where $Sh = K_B L/D$, $Re_L = LV^\infty/\nu$, and $K_B =$ either K_L or K_G. The analogy is as follows: If equation (8.44) works for laminar flows, why not try it for the mass transfer from a solid surface into a turbulent boundary layer? Only the power on the Reynolds number will be changed, through a fit of the following equation to experimental data:

$$Sh = \alpha_0\ Re^{\alpha_1}\ Sc^{1/3} \tag{8.45}$$

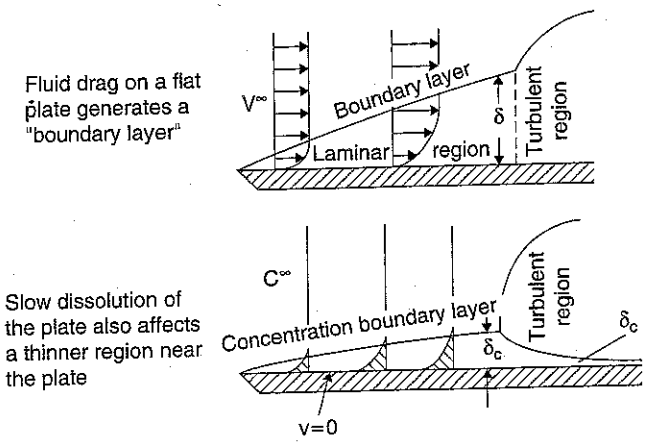

Figure 8.11. Illustration of a boundary layer and a concentration boundary layer on a flat plate. (Adapted from Cussler, 1997.)

where α_0 and α_1 are coefficients to be determined. This is, for the most part, how the characterization equations have been developed in the literature. Table 4.2 provides a number of these equations.

E. Solution of Diffusion Equation Near an Interface

In this section, we will leave the conceptual theories behind and progress to fluid transport with turbulence measurements. This technique was developed by Hanratty and coworkers in the 1970s and 1980s (Campbell and Hanratty, 1982; McCready et al., 1986; Sikar and Hanratty, 1970), with some early free-surface analysis performed by Chen and Scriven (1970). Let us consider a wind blowing over a water surface and the water, in turn, moving above a solid surface. We will be considering the transfer of a volatile compound in which the resistance in the water phase will dominate because of the high resistance to mass transfer in the water phase. In addition, the concentration gradient will be in the water phase, as shown in Figure 8.12. We will assign $z = 0$ at the water surface and at the solid surface.

Now, consider the mass transport equation within roughly $2\delta_c$ of the interface, where there is no turbulent transport because $\delta_c \ll \delta$:

$$\frac{\partial C}{\partial t} + u\frac{\partial C}{\partial x} + v\frac{\partial C}{\partial y} + w\frac{\partial C}{\partial z} = D\left(\frac{\partial^2 C}{\partial x^2} + \frac{\partial^2 C}{\partial y^2} + \frac{\partial^2 C}{\partial z^2}\right) \tag{8.46}$$

The gradients in the x- and y-directions are probably small when compared with the large gradient in the z-direction. This will be sufficient to overcome the fact that u and v are greater than w. Thus,

$$w\frac{\partial C}{\partial z} \gg u\frac{\partial C}{\partial x}, \quad v\frac{\partial C}{\partial y} \tag{8.47}$$

and

$$\frac{\partial^2 C}{\partial z^2} \gg \frac{\partial^2 C}{\partial x^2}, \quad \frac{\partial^2 C}{\partial y^2} \tag{8.48}$$

Then, equation (8.46) becomes

$$\frac{\partial C}{\partial t} + w\frac{\partial C}{\partial z} = D\frac{\partial^2 C}{\partial z^2} \tag{8.49}$$

What we have done with equation (8.49) is convert C and w from functions of x, y, z, and t to functions of z and t. In equation (8.49), we then have the parameters $w(z,t)$, $C(z,t)$, and D. The only unknowns are the dependent variable, C, and w, as D can be

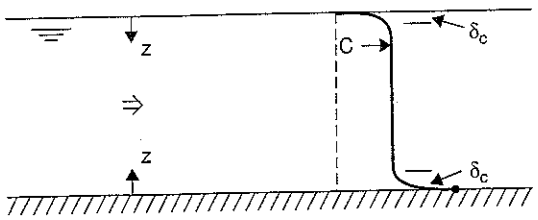

Figure 8.12. Illustration of volatile compound transport from a solid surface and from the water into the air.

determined either from measurements or from the predictive techniques described in Chapter 3. If we can somehow determine $w(z, t)$, we can numerically solve for $C(z, t)$.

In addition, we know these relationships for mass flux:

$$J = -D\frac{\partial C}{\partial z}\Big|_{z=0} = K_L(C^{\infty} - C^{i}) \tag{8.50}$$

Thus, if we can determine $C(z, t)$, we can also apply equation (8.50) to find $K_L(t)$, and

$$\overline{K_L} = \frac{1}{\Delta t}\int_{\Delta t} K_L(t)dt \tag{8.51}$$

We now have the following recipe to determine $K_L(t)$ and $\overline{K_L}$:

1. Given D, measure $w(z,t)$ within $2\delta_c$ of the interface.
2. For given boundary conditions, such as $C^I = C^*$ and $C^{\infty} = 0$, solve equation (8.49) numerically for $C(z,t)$ and $\partial C/\partial z(t)$ at $z = 0$.
3. Solve equation (8.50) for $K_L(t)$.
4. Solve equation (8.51) for $\overline{K}_L$.

Note that our recipe does not require measurement of any concentration – that is because $K_L = K_L(D, \text{turbulence})$. K_L is *not* a function of concentration. It is thus logical that we do not have to measure concentration to measure K_L, as long as we know the fundamental relation between turbulence and mass transfer. Of course, there are difficulties with this four-step recipe. Primarily, item 1: "Measure $w(z,t)$ within $2\delta_c$ of the interface." In water, a fairly large concentration boundary layer would be 100 μm. How are we going to get a profile of velocity measurements to determine $w(z,t)$ within 200 μm of the interface, when the measuring volumes of most instruments are greater than 200 μm? This is the problem that Thomas Hanratty and coworkers recognized and solved.

Hanratty et al.'s Solution to Recipe Item 1. Recipe item 1 will have a set of substeps that must be undertaken to find a solution to this measurement problem. They are:

1a. Assume that $w(z,t)$ may be separated into two individual functions of time and distance, respectively, or

$$w(z, t) = \beta(t)g(z) \tag{8.52}$$

where $\beta(t)$ is Hanratty's beta, representing the driving turbulence outside of the concentration boundary layer, δ_c, and $g(z)$ represents the stretching, shrinking, and overall dissipation of the turbulent eddies as they approach the interface. These processes are illustrated in Figure 8.13.

1b. Expand $g(z)$ from $z = 0$ to $z = \delta_c$, as in equation (8.53):

$$g(z) = g_0 + g_1 z + g_2 z^2 + \cdots \tag{8.53}$$

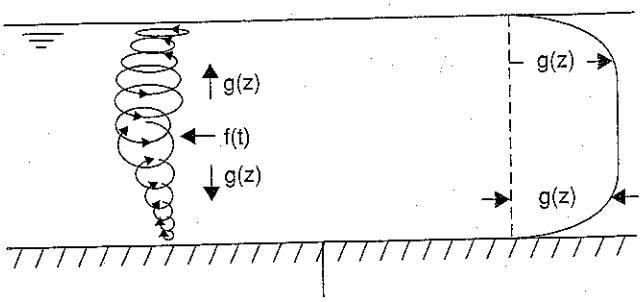

Figure 8.13. Illustration of the two processes represented by $f(t)$ and $g(z)$ in the interface turbulence decomposition of Hanratty and others.

1c. Apply continuity at the interface, shown in equation (8.54):

$$\frac{\partial w}{\partial z} = \frac{\partial g}{\partial z}\beta(t) \tag{8.54}$$

We now need to determine $\partial u/\partial x$ and $\partial v/\partial y$ in equation (8.54). This will be accomplished in steps 1d, 1e, and 1f.

1d. Expand u and v about the interface ($z = 0$). Then,

$$u(x, y, z, t) = \sum_{k=0}^{\infty}\sum_{j=0}^{\infty}\sum_{i=0}^{\infty}\phi_{i,j,k}x^i y^j z^k \tag{8.55}$$

and

$$v(x, y, z, t) = \sum_{k=0}^{\infty}\sum_{j=0}^{\infty}\sum_{i=0}^{\infty}\eta_{i,j,k}x^i y^j z^k \tag{8.56}$$

where φ and η are both some function of time. Equations (8.55) and (8.56) do not truly need to be evaluated to $(i, j, k) = \infty$, because we are actually very close to $z = 0$, and the higher order terms will not be significant. Applying the summations for 0 and 1, for example, is sufficient, and results in four terms in equations (8.55) and (8.56).

1e. Apply the boundary conditions at $z = 0$. For a free interface, these are $w = 0$, $\partial u/\partial z = 0$, and $\partial v/\partial z = 0$. At a fixed interface, the boundary conditions are $w = 0$, $u = 0$, and $v = 0$.

1f. Solve equations (8.53) through (8.56) for $g(z)$. The result of this operation is different for a *free interface*, given in equation (8.57),

$$w = \beta(t)z \tag{8.57}$$

than the result for a *fixed interface*, given in equation (8.58):

$$w = \beta(t)z^2 \tag{8.58}$$

The difference between a free interface (equation (8.57)) and a fixed interface (equation (8.58)) will eventually result in a different dependence of K_L on diffusion coefficient.

Campbell and Hanratty (1982) used Lau's (1980) measurements with some special optics on a laser Doppler velocimetry system to calculate $\beta(t)$ near a fixed interface, in this case, the inside of a clear pipe. They determined $w(z,t)$ from equation (8.52), and solved equations (8.49) and (8.50) numerically for $K_L(t)$. Finally, they applied equation (8.51) to determine K_L, which has been the goal all along. The end results (K_L) may then be related to the other, independent parameters that are important to the transfer process, such as diffusivity, viscosity, and turbulence parameters. Campbell and Hanratty performed this operation and found the following correlation:

$$K_L = u_* F[\beta(t)] Sc^{-7/10} \tag{8.59}$$

or

$$Sh = F[\beta(t)] Re_* Sc^{0.3} \tag{8.60}$$

where F is a function that uses the frequency spectra of $\beta(t)$.

$$F[\beta(t)] = 0.237 S_{\beta m}^{+0.21} \tag{8.61}$$

where $S_{\beta m}^{+} = S_{\beta m} \nu / u_*^2$ and $S_{\beta m}$ is the maximum value of the frequency spectrum of β with units of time^{-1}. Note that equation (8.60) is proportional to $Sc^{0.3}$, rather that $Sc^{1/3}$ for the fixed interface. $Sc^{1/3}$ was based on an *analogy* to a laminar boundary layer, which worked fairly well for fixed interfaces but was not necessarily correct for a turbulent boundary layer. The correlation of Campbell and Hanratty (1982) was based on actual data and on numerical simulations over the range of relevant conditions. It is likely that the 0.3 power relationship is the correct one.

So, now that we have the fixed interface fairly well described, what about the free interface? This actually presents another problem for the techniques of Campbell and Hanratty. The $z = 0$ axis is *on* the water surface. If the water surface moves up and down, the axis moves with it, and is actually a moving coordinate system. It is difficult to get a water surface, exposed to turbulence, that does not move more than 100 μm.

McCready et al. (1986) assumed that the turbulence that was measured by Campbell and Hanratty near a fixed interface could also be applied to a free interface (i.e., $f(t)$ could be the same); it was only $g(z)$ that would be different. Thus, the same velocity measurements were applied to a free surface. The results of the numerical analysis were quite different and are given in equations (8.62) and (8.63).

$$K_L = (0.5 \beta_{\text{rms}} D)^{1/2} \tag{8.62}$$

or

$$Sh_* = 0.71\ Sc^{1/2} \beta^{+1/2} Re_* \tag{8.63}$$

where $\beta_{\text{rms}} = [\overline{\beta(t)^2}]^{1/2}$ is the root mean square value of β, and $\beta^+ = \beta_{\text{rms}} \nu / u_*^2$. McCready et al. used a linear approach applied to equation (8.49) to explain the parameterization differences between equations (8.59) through (8.61) and equation (8.63): if all of the scales of β are important to gas transfer, then β_{rms} is the independent parameter to characterize K_L. If only the larger scales of β are important, then $S_{\beta m}$ is the parameter that should be in the characterization.

From equation (8.62), we can see that we also have a "measurement" of the surface renewal rate, r:

$$r = 0.5\beta_{\text{rms}} \tag{8.64}$$

The penetration and surface renewal theories started out as conceptual, in that they were visualized to occur as such by individual theorists. These theories appeared to work successfully for a free interface, such as the air–water interface, but not for a fixed interface, such as solid–water. Now, the explanation is before us in equation (8.64). Surface renewal is a fairly accurate representation of Hanratty's β at a free surface, and therefore can be seen to give representative results. It is Hanratty's β that we really should be measuring, and it happens that the mean surface renewal rate is a good representation of Hanratty's β at a free surface.

Attempts were made to visualize and measure these surface renewal events on a free surface (Davies and Khan, 1965; Gulliver and Halverson, 1989; Komori et al., 1982; Rashidi and Banerjee, 1988), but measurements were still concentrating on a parameter from a conceptual theory, with no ability to distinguish if it was truly related to K_L. Tamburrino and Gulliver (1994, 2002) developed a means of visualizing and measuring Hanratty's β through streakline imaging or particle tracking velocimetry on a water surface that is close to horizontal to the camera. Applying continuity to equation (8.57) at the free surface:

$$\beta = -\left(\frac{\partial u}{\partial x} + \frac{\partial v}{\partial y}\right) \tag{8.65}$$

Equation (8.65) tells us that if we can measure the two-dimensional divergence on a free surface, then we are also measuring Hanratty's β. A sample of these types of results, given in Figure 8.14, indicates that the scale of Hanratty's β is a fraction of that associated with lower frequency events. This means that virtually all of the measurements of surface renewal have proven to be measuring something else, because they concentrated on the low-frequency events. On a laboratory scale, we are currently able to take measurements of two-dimensional divergence that can be used to describe the liquid film coefficient directly through equations like equation (8.62).

Other measurements of Hanratty's β have been made or inferred from various techniques, including a hot film probe just under the water surface (Brumley and Jirka, 1987), particle image velocimetry in a vertical laser sheet leading up to the water surface with a florescent dye to indicate water surface location accurately (Law and Khoo, 2002) and PIV on the water surface (McKenna and McGillis, 2004; Orlins and Gulliver, 2002). The measurements of Law and Khoo (2002) are especially interesting because the following relationship was developed from experiments on both a jet-stirred tank and a wind–wave channel:

$$K_L = (0.05 D\beta_{\text{rms}})^{1/2} \tag{8.66}$$

or

$$Sh = 0.22\ Sc^{1/2}\beta^{+1/2}\ Re \tag{8.67}$$

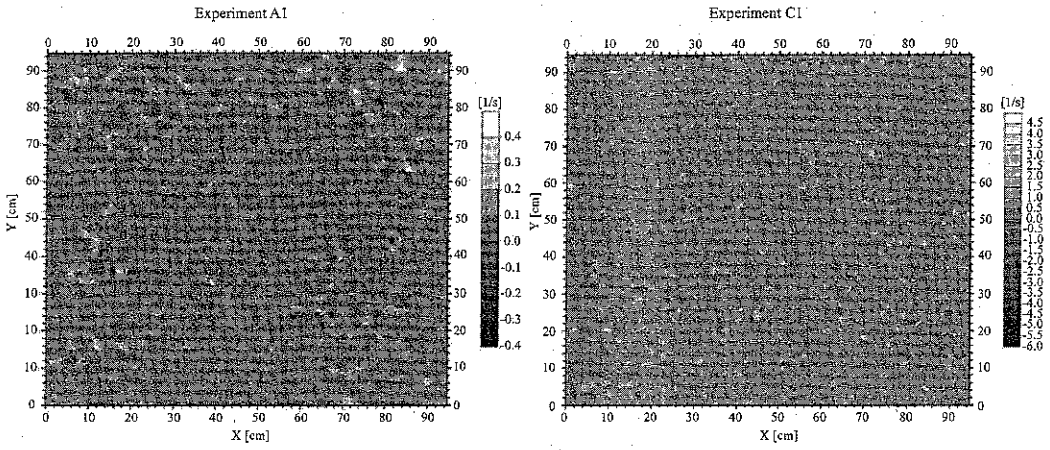

Figure 8.14. Measurements of Hanratty's β in a 95-cm tank stirred by jets emanating from the bottom. *Left* and *right* images are at depths of 44 cm and 22 cm, respectively (Adapted from Tamburrino and Aravena, 2000).

where any convenient turbulence length and velocity scale may be used to make the parameters nondimensional, as long as it is similar for each dimensionless number. The similarities between equations (8.66) and (8.62) are striking, as are the differences. The two equations result in a similar form for the K_L relationship. However, McCready et al. ended up with a coefficient for the equivalent renewal rate of 0.5, while Law and Khoo ended up with 0.05.

In contrast, Tamburrino and Gulliver (2002) related liquid film coefficient from Gulliver and Halverson (1989) and Lau (1975) to their measurements of Hanratty's β for open-channel flows in a flume. They could not get a $K_L \sim \beta_{\text{rms}}^{1/2}$ relationship. Instead, their result was the following:

$$Sh = Sc^{-1/2} \left(\beta^+ Pe_*^2\right)^{0.645} \tag{8.68}$$

where $Pe_* = u_* H/v$. The exponent of 0.645 in equation (8.68) is a problem because the relation for K_L now depends on the turbulence velocity and length scales chosen, which should be avoided with this fundamental approach. Law and Khoo's experiment had higher values of β, which may explain the difference. Tamburrino and Gulliver's hypothesis was that, because the turbulence originated from the channel bottom and went through transitions as it moved to the water surface, the larger β scales had the primary influence on gas transfer coefficient. They computed the frequency spectra of β, verified that their supposition was true, and found the following relationship that gave a dimensionally correct relationship:

$$K_L = (0.058\, S_{\beta m} D)^{1/2} \tag{8.69}$$

or

$$Sh = 0.24\, Sc^{1/2} S_{\beta m}^{+} Re \tag{8.70}$$

Again, any turbulence velocity and length scale are sufficient to use in these dimensionless parameters, as long as they are used in all parameters. Tamburrino and Gulliver used the bottom shear velocity and channel depth. Equation (8.69) provides a measure of surface renewal rate:

$$r = 0.058\ S_{\beta m} \tag{8.71}$$

So, this fundamental approach to determining gas transfer coefficient is still sorting out which flows have all scales contribute to gas transfer coefficient, such that $K_L \sim \beta_{\text{rms}}^{1/2}$, and which flows have only the larger scales of β contribution, such that $K_l \sim S_{\beta m}^{1/2}$. It will be some time before the approach is taken to the field.

F. Gas Film Coefficient

The gas film coefficient is dependent on turbulence in the boundary layer over the water body. Table 4.1 provides Schmidt and Prandtl numbers for air and water. In water, Schmidt and Prandtl numbers on the order of 1,000 and 10, respectively, results in the entire concentration boundary layer being inside of the laminar sublayer of the momentum boundary layer. In air, both the Schmidt and Prandtl numbers are on the order of 1. This means that the analogy between momentum, heat, and mass transport is more precise for air than for water, and the techniques applied to determine momentum transport away from an interface may be more applicable to heat and mass transport in air than they are to the liquid side of the interface.

There are two types of convection in an air boundary layer: (1) forced convection created by air movement across the water body and (2) free convection created by a difference in density between the air in contact with the water surface and the ambient air. If the water body is warmer than the surrounding air, free convection will occur. The combination of these two processes is illustrated in Figure 8.15.

The gas film coefficient due to *free convection* (Figure 8.15a) is described by the relation of Shulyakovskyi (1969):

$$K_G = 0.14\left(\frac{g\alpha_a^2\beta_T\Delta\theta_v}{\nu_a}\right)^{1/3} \quad \text{Positive } \Delta\theta_v \tag{8.72}$$

where g is the acceleration of gravity, α_a is the thermal diffusion coefficient in air, $\beta_T(1/^\circ)$ is the coefficient of thermal expansion for moist air, ν_a is the kinematic viscosity of air, and $\Delta\theta_v$ is the virtual temperature difference between air at the water surface and the ambient air, representing a density difference. Virtual temperature is the density of dry air at otherwise similar conditions. The relation for $\Delta\theta_v$ is:

$$\Delta\theta_v = \left\| T_s\left(1 + 0.378 p_{vs}/P_a\right) - T_a\left(1 + 0.378 p_{va}/P_a\right), 0 \right\| \tag{8.73}$$

where $\|\|$ stands for the greater of the two terms in brackets; T_s and T_a are the temperatures of the water surface and ambient air, respectively; p_{vs} and p_{va} are the vapor pressures of saturated air on the water surface and ambient air, respectively; and P_a is the air pressure.

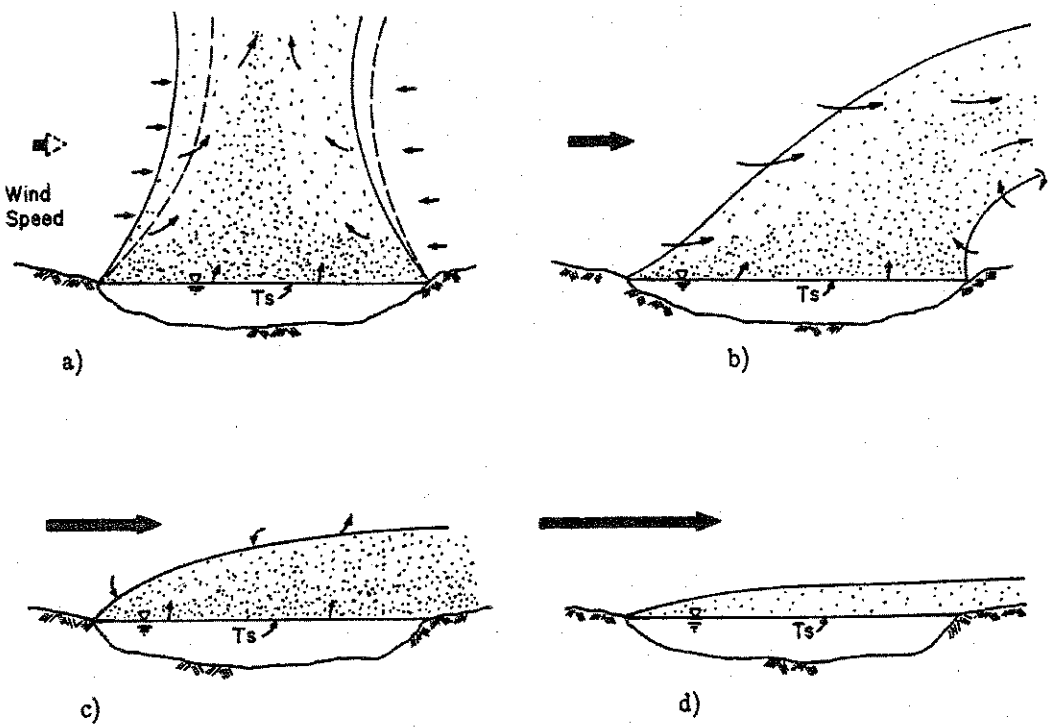

Figure 8.15. Free and forced convection regimes: (*a*) free convective plume, where $T_s > T_{air}$; (*b*) convective plume deflected by wind; (*c*) unstable boundary layer; and (*d*) stable or neutral boundary layer, where $T_s < T_{air}$ (Adams et al., 1990).

Saturation vapor pressure at any air temperature may be computed by the Magnus-Tetons formula:

$$p_{vs}(mb) = 6.11 \exp\left\{\frac{17.3[T(°\text{K}) - 273]}{T(°\text{K}) - 35.9}\right\} \tag{8.74}$$

and atmospheric vapor pressure can be computed from the saturation vapor pressure and relative humidity, RH:

$$p_{va} = \frac{RH}{100} p_{vs} \tag{8.75}$$

Because values of α_a and υ_a can be found from tables such as those in the *Handbook of Chemistry and Physics* (CRC, 2005), all that remains is to determine β_T before we can estimate K_G from free convection. The equation

$$\beta_T = \frac{1}{T_{av}(°\text{C}) + 273} \tag{8.76}$$

will provide us with this parameter, where $T_{av} = T_a(1 + 0.378 p_{va}/P_a)$ is the virtual temperature of the air.

Adams et al. (1990) have investigated the application of the free convection relationships for the cooling water pond at the Savannah River thermal power plant and found that free convection should dominate at wind speeds (at 2 m height) of less than 0.5 – 1 m/s. At wind speeds greater than 1 to 1.5 m/s, the evaporation regime

is that of an unstable forced convective layer, illustrated in Figure 8.15c. Thus, the deflected plume, Figure 8.15b, is a transition regime that will be "smoothed over" for evaporation from water bodies. A stable boundary layer occurs when equation (8.73) is equal to zero.

The *unstable boundary layer* is a flow regime that exists at wind speeds greater than approximately 1.5 m/s when $\Delta\theta_v$ is positive. This is a commonly occurring regime in environmental flows. We will start by assuming the common logarithmic velocity profile in the air boundary layer, altered by a stability function (Brutsaert, 1982) and assign $J_m = \rho u_*^2$ to be the flux of momentum at height z. Then, the momentum/unit volume difference between heights z and $z = 0$ is

$$\rho\,[u(z) - u(z=0)] = \frac{J_m}{\kappa u_*}\left[\ln\left(\frac{z}{z_{0m}}\right) - \psi_m\right] = \frac{u_*}{\kappa}\left[\ln\left(\frac{z}{z_{0m}}\right) - \psi_m\right] \tag{8.77}$$

where $\kappa \approx 0.4$ is von Karmon's constant; z_0 is dynamic roughness, which is a fraction of the true surface roughness (Turner, 1994); and ψ_m is a momentum-flux stability function that is nonzero with stable and unstable boundary layers. For unstable boundary layers, ψ_m is given by (Brutsaert, 1982):

$$\psi_m = \ln\left[\frac{1+(1-16z/L)^{1/2}}{1+(1-16z_{0m}/L)^{1/2}}\right] + 2\ln\left[\frac{1+(1-16z/L)^{1/4}}{1+(1-16z_{0m}/L)^{1/4}}\right] - 2\arctan\left[(1-16z/L)^{1/4}\right] + 2\arctan\left[(1-16z_{0m}/L)^{1/4}\right] \tag{8.78}$$

and L is Obukhov's stability length,

$$L = -\frac{u_*^3}{\kappa B} \tag{8.79}$$

where B is the buoyancy flux per unit area, expressed as

$$B = \frac{g\beta_T(\varphi_c + 0.07\varphi_e)}{\rho C_p} \tag{8.80}$$

where ρ is the density of air, C_p is the specific heat capacity of dry air, φ_c is the heat flux across the water surface by conduction, and φ_e is the evaporative heat flux from the water surface. Equation (8.78) results from the integration of a relatively simple equation curve fit to field data. The integration results in this complicated equation. For a smooth surface, $u_* z_{0m}/\upsilon$ and $u_* z_{oA}/D_A$ are both equal to 9.6. At most wind velocities and wind fetches, however, the water surface is not hydrodynamically smooth, and another relation is needed.

The equation for mass flux of compound A, J_A, and mass of A per unit volume will be written by analogy to equation (8.77):

$$C_A(z) - C_A(z=0) = \frac{J_A}{\kappa u_*}\left[\ln\left(\frac{z}{z_{0A}}\right) - \psi_A\right] \tag{8.81}$$

where ψ_A is given by (Brutsaert, 1982):

$$\psi_A = 2\ln\left[\frac{1+(1-16z/L)^{1/2}}{1+(1-16z_{0A}/L)^{1/2}}\right] \tag{8.82}$$

If equations (8.77) and (8.81) are combined to eliminate shear velocity, an equation can be developed for the flux of compound A:

$$J_A = \frac{\kappa^2 [C_A(z) - C_A(z=0)]\,[u(z) - u(z=0)]}{\left[\ln\left(\frac{z}{z_{0A}}\right) - \psi_A\right]\left[\ln\left(\frac{z}{z_{0m}}\right) - \psi_m\right]} \tag{8.83}$$

Equation (8.83) provides us with an expression for the gas film coefficient for an atmospheric boundary layer:

$$K_G = \frac{\kappa^2 [u(z) - u(z=0)]}{\left[\ln\left(\frac{z}{z_{0A}}\right) - \psi_A\right]\left[\ln\left(\frac{z}{z_{0m}}\right) - \psi_m\right]} \tag{8.84}$$

The gas film coefficient and gas flux rate can be estimated through iteration on equations (8.77) through (8.84), if φ_c and φ_e are known, and a good relationship for z_{0m} and z_{0A} is known. Evaporative heat flux can be determined by applying equation (8.83) to water vapor and using the relationship

$$\varphi_e = L_v J_{H_2O} \tag{8.85}$$

where L_v is the latent heat of vaporization, given as

$$L_v(\text{cal/g}) = 597 - 0.571 T_s(^\circ\text{C}) \tag{8.86}$$

where T_s is water surface temperature. Then, Bowen's ratio (Bowen, 1926) may be used to compute φ_c:

$$\varphi_c = 0.61 P_a(\text{bars}) L_e K_G [T_s - T(z)] \tag{8.87}$$

where P_a is air pressure. The application of these equations to determine gas film coefficient will be demonstrated in Example 8.6.

EXAMPLE 8.6: *Computation of gas film coefficient over a water body*

Long lake, with a fetch of 10 km, is exposed to various wind speeds. On a cold day in fall, the water temperature at 10°C has not cooled yet, but the air temperature is at −5°C. The relative humidity is 100%. Compute the gas film coefficient for water vapor at various wind fetch lengths for wind speeds at 2 m height, between 2 and 20 m/s.

For these conditions, we have the following water vapor concentrations:

$C_{H_2O}(z=0) = p_{vs}\rho/P_a = 13\,\text{g/m}^3$, assuming that $P_a = 1.013$ bars, and,
$C_{H_2O}(z) = 4\text{g/m}^3$

In addition, we need to find a parametric relationship for z_0, which will be equal to z_{0H_2O} at velocities above 2 m/s, because the boundary of the water surface will

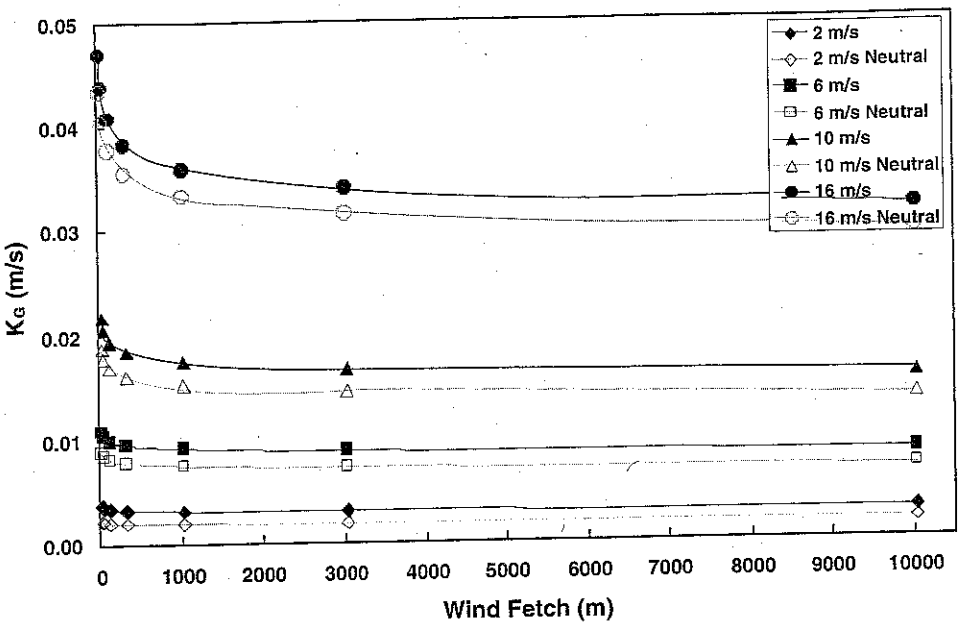

Figure E8.6.1. Computations of gas film coefficient for the unstable boundary layer of Example 8.6 and for a neutral boundary layer that is otherwise similar.

be rough. Gulliver and Song (1986) combined the relationships of Hsu (1974) and Mitsuyatsu (1968) for gravity waves to get

$$\frac{z_0 g}{u_*^2} = 0.00942\pi \left(\frac{gF}{u_*^2}\right) \tag{E8.6.1}$$

and the relations of Hsu and Long and Hwang (1976) for capillary waves to get

$$\frac{z_0 g}{u_*^2} = 0.0219\pi \left(\frac{gF}{u_*^2}\right)^{1/2} \left(\frac{\sigma}{\rho g F}\right)^{1/3} \tag{E8.6.2}$$

where σ is the surface tension of clean water exposed to air. The transition is presumed to occur when z_0 from equation E8.6.2 becomes greater than that of equation (E8.6.1). Finally, Wu (1975) gives

$$u(z=0) = 0.55 u_* \sqrt{\frac{\rho}{\rho_w}} \tag{E8.6.3}$$

where ρ_w is the water density.

We will assume that $z_{0m} = z_{0A} = z_0$, which is generally true except for a smooth water surface. When we use equations (E8.6.1) through (E8.6.3), along with the equations provided above (8.77) through (8.87) to compute K_G for water vapor versus fetch for different wind velocities, the result is that provided in Figure E8.6.1. Iteration was required on the entire set of equations. Also provided in Figure E8.6.1 are similar results for neutral conditions, with $\psi_m = \psi_{H_2O} = 0$. The gas film coefficient decreases with fetch length as z_0 decreases due to an increase in wave velocity. Even though the water surface is not moving quickly, as equation (E8.6.3) can be used to

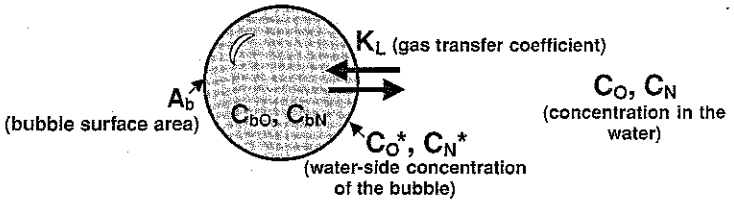

Figure 8.16. Parameters important to the bubble–water gas transfer.

demonstrate, the waves that provide the roughness are moving faster as the wind fetch increases.

G. Bubble–Water Gas Transfer

Bubbles complicate the mass transfer process because the concentration of gases in the bubble is not constant with time. Instead of being exposed to the atmosphere – which is assumed to be a large container such that ambient concentrations do not change in the time of interest – a bubble volume is more limited, and the concentration of the various compounds can change due to mass flux or due to a change in pressure. This means that, for a volatile compound (for a gas), the equilibrium concentration at the water surface is not constant.

We will perform a mass balance on oxygen, which is commonly of interest in bubble–water gas transfer and is illustrated in Figure 8.16. Bubbles are often placed into the water because of their high surface area and tendency to generate their own turbulence. A similar mass balance may be performed on any compound in the water or the gas in the bubbles. Air is mostly oxygen and nitrogen, as given in Table 8.3, with a smaller concentration of argon and traces of other compounds. Humid air, such as air bubbles, also needs to incorporate water vapor using equation (8.74) and the relation

$$C_{H_2O}(\%) = \frac{p_{vs}}{P_a} \tag{8.88}$$

Table 8.3: *Composition of dry air (CRC, 2005)*

Gas	Symbol	% by volume	% by mass	Molecular weight
Nitrogen	N_2	78.08	75.47	28.01
Oxygen	O_2	20.95	23.20	32.00
Argon	Ar	0.93	1.28	39.95
Carbon dioxide	CO_2	0.038	0.0590	44.01
Neon	Ne	0.0018	0.0012	20.18
Helium	He	0.0005	0.00007	4.00
Krypton	Kr	0.0001	0.0003	83.80
Hydrogen	H_2	0.00005	Negligible	2.02
Xenon	Xe	8.7×10^{-6}	0.00004	131.30

Then, to keep the total at 100%, other gas concentrations need to be adjusted accordingly.

We will conserve both nitrogen and oxygen gas. Often, argon is considered to be similar to nitrogen because both are nonreactive and have close to the same diffusion coefficient. Because both gases are volatile, there is no significant resistance on the gas side of the interface, and

$$C_{bO} = H_O C_O^* \tag{8.89a}$$

$$C_{bN} = H_N C_N^* \tag{8.89b}$$

Then, the change of concentration in the water phase is given by

$$V\frac{dC_O}{dt} = K_{LO}A_b\,(C_O^* - C_O) + K_{LSO}A_s\,(C_{sO} - C_O) \tag{8.90a}$$

and

$$V\frac{dC_N}{dt} = K_{LN}A_b\,(C_N^* - C_N) + K_{LSN}A_s\,(C_{SN} - C_N) \tag{8.90b}$$

where V is the volume of water; subscripts N and O indicate nitrogen and oxygen compounds, respectively; K_L is the liquid film coefficient; K_{LS} is the liquid film coefficient of the water exposed to the atmosphere; A_b is the bubble surface area; A_s is the surface area exposed to the atmosphere; C is the water-side concentration; C^* is the concentration of the water in equilibrium with the bubble; and C_S is the saturation concentration of water exposed to the atmosphere. For bubbles greater than approximately 0.5 mm in diameter, the bubble surface acts similar to a free surface because of the toroidal circulation of gas inside of the bubble, as illustrated in Figure 8.17. Then, equation (8.62) applies:

$$K_{LSN} = \left(\frac{D_N}{D_O}\right)^{1/2} K_{LSO} \tag{8.91a}$$

$$K_{LN} = \left(\frac{D_N}{D_O}\right)^{1/2} K_{LO} \tag{8.91b}$$

where D is the diffusion coefficient of the compound in water. For bubbles less than approximately 0.5 mm in diameter, the bubble acts similar to a solid and equation (8.59) applies. This gives

$$K_{LN} = \left(\frac{D_N}{D_O}\right)^{0.3} K_{LO} \tag{8.92}$$

The concentration inside of the bubble must also be considered:

$$V_b\frac{dC_{bO}}{dt} = K_{LO}\,(C_O^* - C_O) \tag{8.93a}$$

$$V_b\frac{dC_{bN}}{dt} = K_{LN}\,(C_N^* - C_N) \tag{8.93b}$$

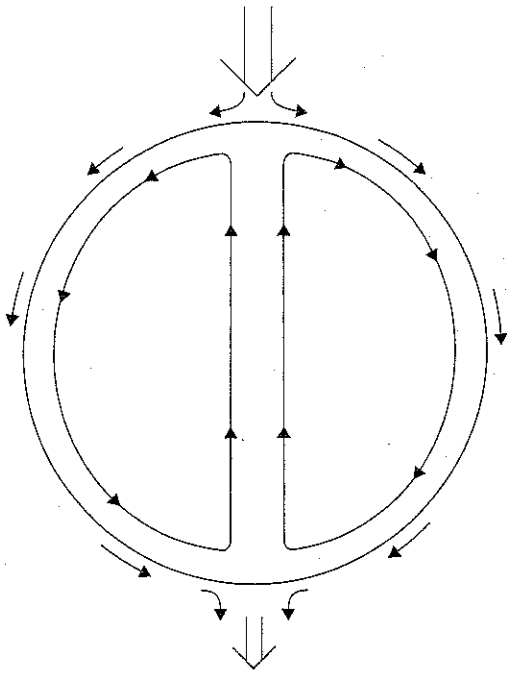

Figure 8.17. Circulation of gas inside of a bubble. The coordinate system is moving with the bubble.

where V_b is the volume of the bubble and C_b is the concentration of the respective compound in the bubble. Because of the difference in pressure that a bubble experiences, it is easier to keep track of the mole ratio, y_m:

$$y_m = \frac{C_{bO}}{C_{bN}} \tag{8.94}$$

where concentration is given in moles/volume, and

$$\frac{dy_m}{dt} = \frac{\partial y_m}{\partial t} + v_r \frac{\partial y_m}{\partial z} \tag{8.95}$$

where v_r is the rise velocity of the bubble. The $\partial y_m/\partial t$ term can be visualized as the change of y_m over time at one location, with many bubbles streaming by. This term is generally small compared with the last term in equation (8.95) and will be assumed negligible for the computation of y_m, as long as accurate values of C_O, C_N, etc., are known. We will therefore concentrate on the $\partial y_m/\partial z$ term. Thus,

$$\frac{\partial y_m}{\partial z} = \frac{\partial \left(C_{bO}/C_{bN}\right)}{\partial z} = \frac{1}{C_{bN}} \frac{\partial C_{bO}}{\partial z} - \frac{C_{bO}}{C_{bN}^2} \frac{\partial C_{bN}}{\partial z} \tag{8.96}$$

To determine C_{bO} and C_{bN}, we will return to the mass flux:

$$v_r V_b \frac{\partial C_{bO}}{\partial z} = K_{LO} \left(C_O^* - C_O\right) \tag{8.97a}$$

$$v_r V_b \frac{\partial C_{bN}}{\partial z} = K_{LN} \left(C_N^* - C_N\right) \tag{8.97b}$$

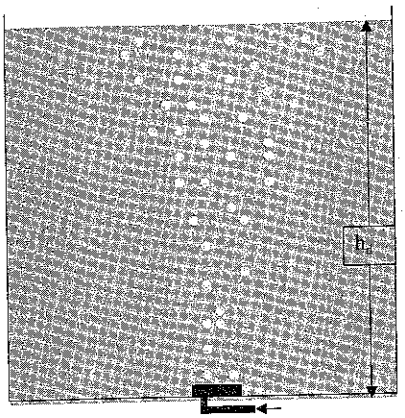

Figure 8.18. Illustration of a bubble plume in a tank.

The terms v_r and V_b are terms that must be estimated. However, the multiplicative pair, $v_r V_b$, can be converted through analysis of a rising bubble plume (McWhirter and Hutter, 1989), as shown in Figure 8.18. The residence time of bubbles in the tank, t_r, is given by $t_r = V_b/Q_a$, where Q_a is the discharge of air into the tank. In addition, $t_r = h_d/v_r$, where h_d is the depth of water in the tank. Then,

$$t_r = \frac{V_b}{Q_a} = \frac{h_d}{v_r} \tag{8.98}$$

which means that

$$V_b v_r = Q_a h_d \tag{8.99}$$

Thus, the unknown term in equation (8.97), $V_b\, v_r$, has been replaced with the known terms, $Q_a\, h_d$.

Substituting equation (8.99) into (8.97) gives

$$\frac{\partial C_{bO}}{\partial z} = \frac{K_{LO} A_b}{Q_a h_d} (C_O^* - C_O) \tag{8.100a}$$

$$\frac{\partial C_{bN}}{\partial z} = \frac{K_{LN} A_b}{Q_a h_d} (C_N^* - C_N) \tag{8.100b}$$

Now, substituting equations (8.89), (8.91), and (8.100) into (8.96) gives

$$\frac{\partial y_m}{\partial z} = \frac{-K_{LO} A_b}{h_d Q_a} \left[\frac{1}{H_N C_N^*} (C_O^* - C_O) - \left(\frac{D_N}{D_O} \right)^{1/2} \frac{H_O C_O^*}{(H_N C_N^*)^2} (C_N^* - C_N) \right] \tag{8.101}$$

These equations are finalized by determining the equilibrium concentration between the bubble and the water on the edge of the bubble:

$$C_O^* = C_{SO} \frac{P_a - p_v + [\rho_L g (h_d - z)]}{P_{\text{atm}} - p_v} \frac{y_m}{0.208(1 + y_m)} \tag{8.102a}$$

$$C_N^* = C_{SN} \frac{P_a - p_v + [\rho_L g (h_d - z)]}{P_{\text{atm}} - p_v} \frac{1}{0.208(1 + y_m)} \tag{8.102b}$$

where ρ_L is the density of the liquid, P_a is the pressure of the local atmosphere, p_v is the vapor pressure, and P_{atm} is the pressure of the standard atmosphere. Equation (8.102) changes with depth as z and y_m change with depth. The boundary condition of equations (8.101) and (8.102) is the gas molar ratio at the sparger, which is 0.266 for air and the initial concentrations C_O and C_N in the liquid. The equations are then solved from $z = 0$ to $z = h_d$ at one moment in time and used to compute C_O and C_N in equation (8.90) for the next time step.

We can see that the equations and solution technique have an added degree of complexity for bubble–water gas transfer, primarily because of the variation of pressure and because the gas control volume cannot be considered large. These are, however, simply the mass conservation equations, which should not be considered difficult, only cumbersome. Any reduction of these equations is an assumption, which would need to be justified for the particular application. If transfer of a trace gas is of interest, then similar equations for the trace gas would need to be added to those provided above.

We also need to develop the theories for liquid film coefficient to use in the aforementioned equations. For drops that are close to spherical, without separation, Levich (1962) assumed that the concentration boundary layer developed as the bubble interface moved from the top to the bottom of a spherical bubble. Then, it is possible to use the concepts applied in Section 8.C and some relations for the streamlines around a bubble to determine K_L:

$$Sh = \left(\frac{4}{\pi} Pe\right)^{1/2} \tag{8.103}$$

where $Sh = K_L d_b / D$, $Pe = v_r d_b / D$, and d_b is the bubble diameter. Equation (8.103) should apply as long as the bubble is spherical and the interface moves with the rise of the bubble. For bubbles where the surface acts as a solid surface (does not move), and is spherical, Friedlander (1961) developed the equation

$$Sh = 0.99 Pe^{1/3} \tag{8.104}$$

that applies to very small bubbles. In general, most of the gas transfer is across bubbles that are not spherical, because of turbulence generated in the bubble rise field, so variations on equations (8.103) and (8.104) have been proposed, as given in Table 4.2. These equations, however, do provide a good basis from which to develop characterization equations.

H. Interfacial Transfer with Reaction

There are a number of environmentally significant compounds that undergo a reaction while moving through the water-side, concentration boundary layer, such that the flux rate is altered. If the flux rate is altered, then the apparent rate coefficient is also affected. Typical examples would be the compounds that react with

Table 8.4: *Environmentally significant compounds that react with water*

								$k(s^{-1})$
CO_2	+	H_2O	⇒	H_2CO_3				3.7×10^{-2}
Cl_2	+	H_2O	⇒	HOCl	+	H^+	+ Cl^-	28
H_2S	+	H_2O	⇒	HS^-	+	H_3O^+		$4. \times 10^2$
NH_3	+	H_2O	⇒	NH_4^+	+	OH^-		
CH_3COOH (Methyl formate)	+	H_2O	⇒	CH_3COO^-	+	H_3O^+		$1. \times 10^5$

water, such as the reactions given in Table 8.4. These reactions are all essentially *irreversible.*

EXAMPLE 8.7: *Absorption rate of carbon dioxide by the oceans*

Carbon dioxide is one of the major global warming gases. The ocean acts as a reservoir for carbon dioxide and therefore will slow the effects of this gas on global warming. How is this air–water transfer rate dependent on the rate of reaction of carbon dioxide with liquid water to form H_2CO_3?

Carbon dioxide has a source/sink rate of $-k\,C$, where C is the water concentration of carbon dioxide. The concentration profile in the concentration boundary layer would be steeper near the interface, as illustrated in Figure E8.7.1.

Thus, the diffusion equation within the water concentration boundary layer becomes

$$\frac{\partial C}{\partial t} = D\frac{\partial^2 C}{\partial z^2} - kC \tag{E8.7.1}$$

with boundary conditions:

1. At $t = 0^+, z = 0, C = C_0$
2. At $t = 0, z > 0, C = 0$

The solution to equation (E8.7.1) has been developed by Danckwerts (1970):

$$\frac{C}{C_0} = \frac{1}{2}\exp\left(-z\sqrt{\frac{k}{D}}\right)\operatorname{erfc}\left(\frac{z}{2\sqrt{tD}} - \sqrt{kt}\right) + \frac{1}{2}\exp\left(z\sqrt{\frac{k}{D}}\right)\operatorname{erfc}\left(\frac{z}{2\sqrt{tD}} + \sqrt{kt}\right) \tag{E8.7.2}$$

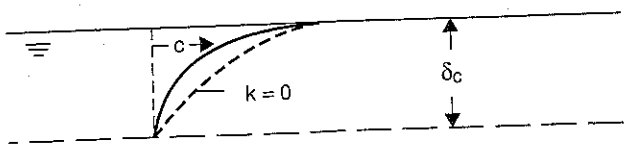

Figure E8.7.1. Concentration profile with a first-order, irreversible degradation reaction (*solid line*) and an equivalent concentration profile without reaction (*dashed line*).

Table E8.7.1: *Transfer enhancement ratio for a range of liquid film coefficients common on the ocean surface*

Wind velocity (m/s):	0.5	1	2	4	6	8	12	16
$\sqrt{kD}/K_L$:	19.7	6.3	2.0	0.7	0.3	0.2	0.1	0.07
K_E/K_L:	19.9	6.5	2.2	1.2	1.2	1.0	1.0	1.0

The flux rate at $z = 0$ is found by the equation

$$J = -D\frac{\partial C}{\partial z}\Big|_{z=0} \tag{E8.7.3}$$

which gives

$$J = C_0\sqrt{kD}\left(\text{erf}\sqrt{\text{kt}} + \frac{e^{-kt}}{\sqrt{\pi\,\text{kt}}}\right) \tag{E8.7.4}$$

From equation (E8.7.4), we can see that an equivalent, bulk, liquid-film coefficient, K_E, would be

$$K_E = \sqrt{kD}\left(\text{erf}\sqrt{kt} + \frac{e^{-kt}}{\sqrt{\pi\,kt}}\right) \tag{E8.7.5}$$

Of course, the concentration boundary layer does not grow indefinitely, but the penetration or the surface renewal theories give us a means of dealing with that fact. If we are going to use the penetration theory, $t \Rightarrow t_e$. If we are going to use the surface renewal theory, $t \Rightarrow 1/\pi r$. With the penetration theory, the transfer enhancement ratio, K_E/K_L, is then given as

$$\frac{K_E}{K_L} = \sqrt{\pi kt_e}\left(\text{erf}\sqrt{\text{kt}_\text{e}} + \frac{e^{-kt_e}}{\sqrt{\pi kt_e}}\right) \tag{E8.7.6}$$

A similar substitution will give the transfer enhancement ratio for the surface renewal theory.

Now, we need to estimate t_e for the ocean, influenced by wind. We will use the empirical equation developed by Wanninkhof (1992):

$$K_L(\text{m/s}) = 1.25 \times 10^{-6}\ W\ (\text{m/s})^{1.64} \tag{E8.6.7}$$

where W is wind velocity at 10 m height. Using equations (E8.6.7) and (8.33), $t_e = D/(\pi K_L^2)$, the transfer enhancement ratios given in Table E8.7.1 were computed. The diffusivity of carbon dioxide is $\sim 1.7 \times 10^{-9}\ \text{m}^2/\text{s}$, using the predictive techniques in Chapter 3. A significant enhancement of carbon dioxide transfer is apparent at lower wind velocities. The enhancement is minor at wind velocities above 8 m/s, however.

Note that Example 8.7 could have been used for the enhanced transfer of any compound given in Table 8.3. The enhancement ratio is correlated against the ratio, $(kD)^{1/2}/K_L$ in Figure 8.19.

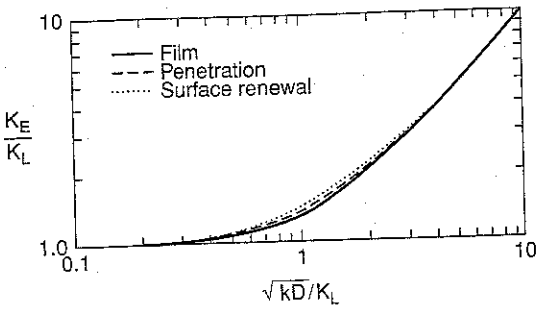

Figure 8.19. The transfer enhancement ratio versus the ratio of $(kD)^{1/2}/K_L$ (Sherwood et al., 1975).

I. Problems

1. (T/F) If a compound is volatile, it will migrate predominately to the air phase.
2. The resistance to mass transfer of a nonvolatile compound is largest in the _____ phase.
3. (T/F) A large Henry's law constant means that the gas is nonvolatile.
4. (T/F) The gas film coefficient is linearly dependent on diffusion coefficient of the compound.
5. Does it make a difference if we use g/m^3 or $moles/m^3$ for Henry's law constant? Why or why not?
6. How would the distribution of mass differ (qualitatively) if DDT were accidentally spilled into the fish tank of Example 8.4 instead of benzene?
7. You have placed an air diffuser (sparger) at the bottom of a 20-m-deep lake for the purpose of increasing oxygen concentrations. The primary cost of spargers is the cost of pressurizing the air to overcome hydrostatic pressure and head losses. The bubbling action adds oxygen to the water through air bubble–water transfer and also through surface air–water transfer. A steady-state water concentration is reached. Is this steady concentration at equilibrium? Why?
8. Consider Example 8.5, except with (a) toluene (a volatile compound) and (b) trichloromethane (a semivolatile compound) added to the water, instead of toxaphene. Sketch the concentration profiles that would be expected at some point in time.
9. What are the boundary conditions in the environment to which the stagnant film, penetration, surface renewal theories, and laminar boundary layer analogy should be applied? Briefly explain why.
10. Sketch a boundary layer profile for momentum, heat, and mass that would occur in the air and in the water. Explain any differences.
11. A rapid reaction in one phase can increase the overall mass transfer rate. Discuss the influence that bubble size might have on the relative importance of a liquid-phase, rapid reaction on mass transfer rate.

9 Air–Water Mass Transfer in the Field

The principles of air–water mass transfer are often difficult to apply in field measurements and thus also in field predictions. The reasons are that the environment is generally large, and the boundary conditions are not well established. In addition, field measurements cannot be controlled as well as laboratory measurements, are much more expensive, and often are not repeatable.

Table 9.1 lists some of the theoretical relationships from Chapter 8, for example, and the difficulties in applying these relationships to field situations. Eventually, application to the field comes down to a creative use of laboratory and field measurements, with a good understanding of the results that theory has given us and to make sure that we do not violate some of the basic principles of the theoretical relationships.

The value of β has not been attempted in the field to date. So, how do we determine K_L for field applications? The determination of dynamic roughness, z_0, has also been difficult for water surfaces. The primary method to measure K_L and K_G is to disturb the equilibrium of a chemical and measure the concentration as it returns toward either equilibrium or a steady state. Variations on this theme will be the topic of this chapter.

A. Gas Transfer in Rivers

1. Measurement of Gas Transfer Coefficient

Rivers are generally considered as a plug flow reactor with dispersion. Determination of the dispersion coefficient for rivers was covered in Chapter 6, and determination of the gas transfer coefficient is a slight addition to that process. We will be measuring the concentration of two tracers: a volatile tracer that is generally a gas (termed a gas tracer, C) and a conservative tracer of concentration (C_c). The transported quantity

Table 9.1: *Theoretical relationships for gas transfer coefficient and the difficulties in applying them in the field*

Theoretical relationship	Difficulties in field application
$J = -D\frac{\partial C}{\partial z}\Big\|_{z\to 0}$	Cannot measure $\partial C/\partial z$ within 100 μm of the free surface
$J = K_L\left(\frac{C_g}{H} - C_w\right)$	Must determine K_L
$J = K_G(C_g - HC_w)$	Must determine K_G
$K_G = \frac{\kappa^2[u(z)-u(z=0)]}{\left[\ln\left(\frac{z}{z_{0A}}\right)-\psi_A\right]\left[\ln\left(\frac{z}{z_{0m}}\right)-\psi_m\right]}$	Do not know z_{0m} or z_{0A}
$K_L = D/\delta$	Do not know $\partial(t, D)$
$K_L = \sqrt{Dr}$	Do not know r
$K_L \approx \sqrt{D\beta_{\text{rms}}}$	Must determine β_{rms}

will be the ratio of the two tracers, $R = C/C_c$. Then, the convection-dispersion equation becomes

$$\frac{\partial R}{\partial t} + \frac{Q}{A_{cs}}\frac{\partial R}{\partial x} = D_L\frac{\partial^2 R}{\partial x^2} + K_L a\,(R_s - R) \tag{9.1}$$

where Q is the river discharge, A_{cs} is the cross-sectional area, $K_L a = K_L A/V = K_2$ is the reaeration coefficient, and a is the specific surface area or surface area per volume of water. If we are oriented in Lagrangian coordinates, the convection term does not appear. In addition, the gradient of the ratio R is presumed to be low, because as the conservative tracer spreads, so will the gas tracer. Finally, most gas tracers do not have a significant concentration in the atmosphere, so $R_s = 0$. Then, equation (9.1) becomes

$$\frac{\partial R}{\partial t} = -K_2 R \tag{9.2}$$

with solution

$$\ln\left(\frac{R_2}{R_1}\right) = -K_2(t_2 - t_1) \tag{9.3}$$

where subscripts 1 and 2 correspond to times 1 and 2. Most gas transfer measurements are made with a dual tracer pulse, in which the pulse requires some distance to mix across the river, as in Chapter 6. Thus, a tracer cloud is followed, and the time is generally taken to be the center of mass of the cloud on which multiple measurements are made. Then, equation (9.4) becomes that which is actually used in practice:

$$K_2 = -\frac{1}{(t_2 - t_1)}\ln\left(\frac{\sum_n R_{2i}}{\sum_n R_{1i}}\right) \tag{9.4}$$

where n is the total number of measurements at a given location. There are other considerations with regard to gas transfer measurements in rivers that are detailed

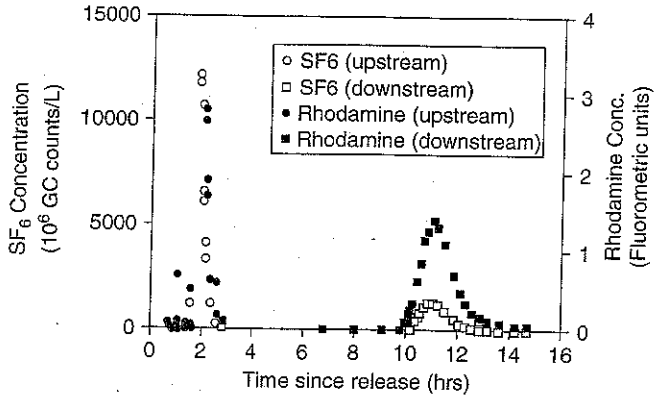

Figure 9.1. Gas tracer pulses for the James River (North Dakota) used to measure the reaeration coefficient. GC, gas chromatograph; SF_6, sulfer hexafloride.

elsewhere (Hibbs et al., 1998; Kilpatrick, 1979). Some typical gas tracer pulses are given in Figure 9.1. These measurements are a significant effort, because one needs to be out for 2 or 3 days and mobilize when the tracer cloud passes, which is usually in the middle of the night.

Of course, the typical objective is the K_2 value for oxygen to be used in such things as total daily maximum load calculations, and we just have the K_2 value for the gas tracer. We can use equation (8.62) to get us from the transfer of one compound to another, because β_{rms} is similar for all compounds:

$$\frac{K_2(\text{O}_2)}{K_2(\text{tracer})} = \left(\frac{D_{\text{O}_2}}{D_t}\right)^{1/2} \tag{9.5}$$

where D_t is the diffusion coefficient of the gas tracer.

2. Prediction of the Gas Transfer Coefficient in Rivers

Measurements of reaeration coefficients have been made at a number of locations over the years, and it is natural that individuals would try to correlate these measurements with the measured parameters of the river so that predictions can be made elsewhere. A partial compilation of measurements is given in Figure 9.2. Although there is scatter in flume measurements, this is exceeded by a factor of 10 in field measurements.

Moog and Jirka (1998) investigated the correspondence of a number of equations with the available data, using the mean multiplicative error, MME:

$$\text{MME} = \exp\left[\frac{\sum_{i=1}^{N} \left|\ln\left(K_p/K_m\right)_i\right|}{N}\right] \tag{9.6}$$

where K_p and K_m are the predicted and measured K_2 values, and N is the number of data. The MME compares the ratio of the prediction with the measurement, so that the study would not be biased toward the higher values of K_2. There are orders

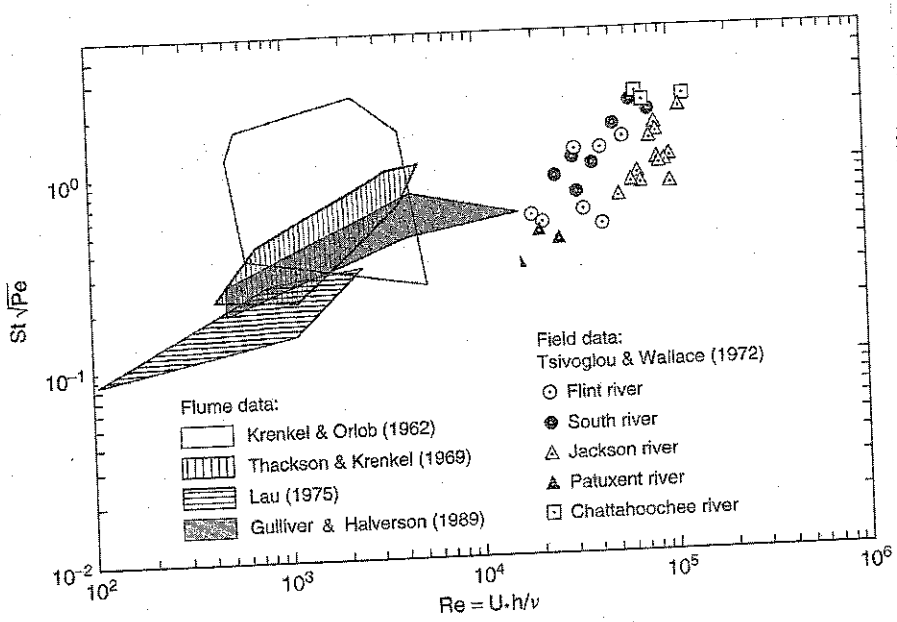

Figure 9.2. Measurements of reaeration coefficient in laboratory flumes and in the field. Present authors are Gulliver and Halverson (1989). *St* is a Stanton number, K_L/u_*.

of magnitude differences in reaeration coefficients, and to simply take the difference between predictions and measurements as the residuals causes the residuals of the larger reaeration coefficients to dominate the process. The MME thus has the following advantages:

1. The small and large values of K_2 are considered equally.
2. The MME is the geometric mean of K_p/K_m. Thus, a given equation is on average, in error by a factor equal to the MME.
3. The MME of K_2 is equal to the MME of K_L. This occurs because the absolute values of the K_p/K_m ratios were utilized, instead of the square of the ratio.

Moog and Jirka then calibrated the lead coefficient and studied the predictive capability of 10 "calibrated" empirical equations to predict reaeration coefficients that were the result of 331 field studies. The result was surprising, because the best predictive equation was developed by Thackston and Krenkel's (1969) from laboratory flume studies, and the comparison was with field equations. In dimensionless form, Thackston and Krenkel's (1969) calibrated (multiplying the lead coefficient by 0.69) equation can be converted to a dimensionless form utilizing Sherwood, Schmidt, Reynolds, and Froude numbers:

$$Sh = 4.4 \times 10^{-3} Sc^{1/2} Re_* \left(1 + F^{1/2}\right) \tag{9.7}$$

where $Sh = K_L h/D = K_2 h^2/D$, $Sc = \nu/D$, $Re_* = u_* h/\nu$, $F = U/\sqrt{gh}$, h is mean stream depth, D is diffusion coefficient of the gas in the water, ν is kinematic viscosity, $u_* = (ghS)^{1/2}$ is shear velocity, S is water surface slope, U is mean stream velocity,

and g is the acceleration of gravity. To convert Thackston and Krenkel's equation to equation (9.7), we have assumed that K_L is proportional to $D^{1/2}$, included the viscosity of water at 20°C, and assumed that $Sc = 476$ for oxygen at 20°C. Equation (9.7) should be functional at all water temperatures in which water is a liquid and for all gases. It is probable that the Froude number in equation (9.7) partially accounts for the additional water surface roughness that occurs above a Froude number of 1.0.

Equation (9.7) results in the following relation for surface renewal rate, r:

$$r = 1.94 \times 10^{-5} \frac{u_*^2}{\nu} \left(1 + F^{1/2}\right) \tag{9.8}$$

Moog and Jirka also found that equation (9.7), even though it was the best predictor, still had an MME of 1.8. This means that one can expect the predictions of equation (9.7) to be off the field measurements by either multiplying or dividing by a factor of 1.8. Fifty percent of the predictions will differ by more than this factor and 50% by less. In addition, they found that below a stream slope of 0.0004, it is just as good to simply use a constant value of K_2 at 20°C of 1.8 days^{-1}, with a 95% confidence interval corresponding to a multiplicative factor of 8. At the low slope values, other factors, such as wind velocity and surfactants on the water surface, could become influencing factors. Considering that there are 331 "high-quality" measurements of reaeration coefficient in streams, with 54 at $S < 0.0004$, we have not made great advances in predicting reaeration coefficient. The obvious question is Why?

There are four possible reasons that will be presented herein. They will be indicative of the difficulties that exist when taking detailed results of experiments and analysis from the laboratory to the field.

1. *Field measurements are not as precise as laboratory measurements.* Although this is a true statement, some dedicated field experimentalists have improved the field techniques greatly over recent decades (Clarke et al., 1994; Hibbs et al., 1998; Kilpatrick et al., 1979; Tsivoglou and Wallace, 1972). Whereas the implementation of field studies is still a challenge, the accuracy cannot account for MME of 1.8.
2. *Turbulence is generated at the channel bottom, and reaeration occurs at the top of the channel.* The importance of turbulence to gas transfer was illustrated in Sections 8.C and 8.D. One confounding experimental problem is that the turbulence is generated at the bottom of the channel and goes through changes in intensity and scale as it moves toward the water surface. This problem exists in both flume and field channel studies, however, and the flume studies are significantly more precise than the field studies.
3. *The independent parameters that are measured are not truly indicative of the important processes for gas transfer.* In Section 8.D, we discussed the revelations of Hanratty and coworkers – that the process important to gas transfer is two-dimensional divergence on the free surface (Hanratty's β):

$$\beta = -\left(\frac{\partial u}{\partial x} + \frac{\partial v}{\partial y}\right) \tag{8.67}$$

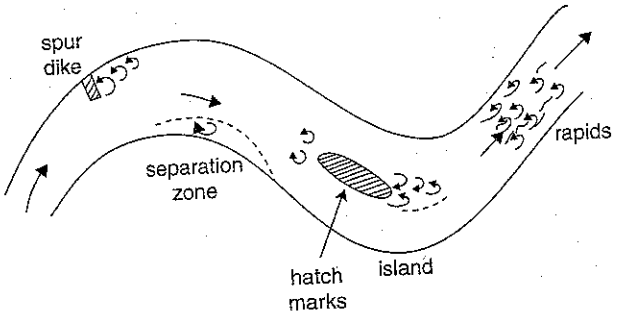

Figure 9.3. Illustration of additional surface vortices in a natural river.

Tamburrino and Gulliver (2002) and Tamburrino and Aravena (2000) have experimentally visualized β on the free surface of turbulent flows and indicated that there is a correlation between β and vorticity, ω, on the free surface:

$$\omega = \frac{\partial u}{\partial y} - \frac{\partial v}{\partial x} \tag{9.9}$$

Now, consider a natural river, illustrated in Figure 9.3. There are many sources of vorticity in a natural river that are not related to bottom shear. Free-surface vortices are formed in front of and behind islands and at channel contractions and expansions. These could have a direct influence on reaeration coefficient, without the dampening effect of stream depth. The measurement of β and surface vorticity in a field stream remains a challenge that has not been adequately addressed.

4. *The mean values that are determined with field measurements are not appropriate.* Most predictive equations for reaeration coefficient use an arithmetic mean velocity, depth, and slope over the entire reach of the measurement (Moog and Jirka, 1998). The process of measuring reaeration coefficient dictates that these reaches be long to insure the accuracy of K_2. Flume measurements, however, have generally shown that $K_2 \sim u*/h$ *or* $K_2 \sim (S/h)^{1/2}$ (Thackston and Krenkel, 1969; Gulliver and Halverson, 1989). If this is truly the case, we should be taking the mean of $S^{1/2}$ and the mean of $h^{-1/2}$ to use the predictive equations to estimate reaeration coefficient. Example 9.1 will investigate whether this is an important consideration.

EXAMPLE 9.1: *Estimation of K_2 using measured independent parameters and two types of mean values*

Most natural rivers and streams are a series of pools and riffles. Calculate the K_2 for one pool riffle pair of equal lengths in a river carrying 12 m^3/s at 20°C, using arithmetic means and the mean values weighted according to equation 9.7. The pool has a width of 60 m, a mean depth of 2 m, and a bottom roughness of 2 mm. The riffle has a width of 10 m, a mean depth of 0.5 m, and is a gravel bottom with 20 mm roughness. No stream slope can be measured over such a short reach.

Equation (9.7) gives us

$$K_2 = 4.4 \times 10^{-3} Sc^{-1/2}(1 + F^{1/2})\frac{u_*}{h} \tag{E9.1.1}$$

Because we do not have the slope to determine u_*, we will use the following equation that results from the definition of the Darcy–Weisbach friction factor:

$$u_* = \sqrt{g R_h S} = \sqrt{\frac{f}{8}} U \tag{E9.1.2}$$

where U is cross-sectional mean velocity and f is the Darcy–Weisbach friction factor. Moody's diagram, given in Appendix A–1, can be used to determine f. We need the Reynolds number, $Re = 4UR_h/\nu$ and the relative roughness, $\varepsilon/4\,R_h$, where $R_h = A/P$ is the hydraulic radius, A is the cross-sectional area, and P is the wetted perimeter. In general, the term $4\,R_h$ takes the place of the diameter in these calculations for noncircular cross sections, because the diameter is equal to $4\,R_h$ in a circular cross section. We will also calculate the mean stream slope, $S = fU^2/(8gR_h)$, rather than the mean shear velocity, because that is what is measured in practice. Then, equation (E9.1.1) becomes

$$K_2 = 4.4 \times 10^{-3} Sc^{-1/2}(1 + F^{1/2})\frac{(gR_hS)^{1/2}}{h} \cong 4.4 \times 10^{-3} Sc^{-1/2}(1 + F^{1/2})\left(\frac{gS}{h}\right)^{1/2} \tag{E9.1.3}$$

and we can calculate the following parameters for the pool and riffle:

Pool	*Riffle*
$U = Q/A = 0.1\,\text{m/s}$	$U = 2.4\,\text{m/s}$
$P = 60 + 4 = 64\,\text{m}$, assuming a rectangular cross section	$P = 11\text{m}$
$R_h = A/P = 1.88\,\text{m}$	$R_h = 0.46\,\text{m}$
$Re = 7.5 \times 10^5$	$Re = 4.4 \times 106$
$\varepsilon/(4R_h) = 2.7 \times 10^{-4}$	$\varepsilon/(4R_h) = 0.010$
$f \sim 0.0155$	$f \sim 0.038$
$S = 0.0155{*}0.1^2/(8{*}9.8{*}1.88) = 1.1 \times 10^{-6}$	$S = 0.038{*}2.4^2/(8{*}9.8{*}.46) = 6 \times 10^{-3}$
$F = 0.1/(9.8{*}1.88)^{1/2} = 0.023$	$F = 2.4/(9.8{*}.46)^{1/2} = 1.13$
$Sc = 1 \times 10^{-6}/2.1 \times 10^{-9} = 476$	$Sc = 476$

We can now use these values to calculate the means and K_2:

Arithmetic mean:

$$S = (1.1 \times 10^{-6} + 6 \times 10^{-3})^{1/2} = 3 \times 10^{-3}$$
$$h = (2 + 0.46)/2 = 1.23\text{m}$$
$$F = (0.1 + 2.4)/2/(9.8 * 1.23)^{1/2} = 0.36$$

Then, equation (E9.1.3) gives

$$K_2 = 9.3 \times 10^{-5}\ \mathrm{s}^{-1}$$

Means weighted according to equation (E9.1.3)

$$S^{1/2} = [(1.1 \times 10^{-6})^{1/2} + (6 \times 10^{-3})^{1/2}]/2 = 3.9 \times 10^{-2}$$
$$S = 1.5 \times 10^{-3}$$
$$1/h^{1/2} = (1/2^{1/2} + 1/0.5^{1/2})/2 = 1.06\ \mathrm{m}^{-1/2}$$
$$h = 0.89\ \mathrm{m}$$
$$F^{1/2} = (0.023^{1/2} + 1.13^{1/2})/2 = 0.61$$
$$F = 0.37$$

and equation (E9.1.3) gives

$$K_2 = 4.2 \times 10^{-5}\ \mathrm{s}^{-1}$$

The difference between the two means is a factor of 2.2. This value is larger than the expected error of equation (9.7). Thus, a channel with a variation in slope and cross section along its length will have a higher K_2 value computed from arithmetic means than an otherwise equivalent channel that does not have variation in slope and cross section. It may not be a coincidence that Moog and Jirka's "calibration" of Thackston and Krenkel's equation for flumes is an adjustment by a factor of 0.69 to represent field measurements. We need to pay attention to the impact that these variations in natural rivers and streams have on our predictive equations for K_2.

The ramifications of the poor K_2 predictive ability are that we cannot do an adequate job of planning for oxygen concentrations during low flow events or for spills, unless we have performed field measurements of reaeration coefficient. This will be explored in Example 9.2.

EXAMPLE 9.2: *Use of predictive relations to determine river withdrawals after a spill*

The Maipo River in central Chile runs past a metal finishing plant in the town of Puente Alto, where 100 kg of carbon tetrachloride (CCl_4) are accidentally spilled into the river. Other compounds were also included in the spill, but the environmental health officials are most concerned about the CCl_4. They have decided that all water supply plants on the river should be shut down if the concentration of the pulse is greater than 5 ppb. At what time and how far downstream will this occur?

In this reach, on the day of the spill, the Maipo River carried a discharge of 60 m^3/s, at a mean depth of 2 m, with a mean cross-sectional area of 60 m^2 and a stream slope of 0.002. The longitudinal dispersion coefficient is known to be 20 m^2/s.

The mass transport equation for this problem is as follows:

$$\frac{\partial C}{\partial t} + \frac{Q}{A_{cs}}\frac{\partial C}{\partial s} = D_L\frac{\partial^2 C}{\partial s^2} - K_2 C \qquad \text{(E9.2.1)}$$

where C is the concentration of CCl_4, Q is river discharge, A_{cs} is cross-sectional area, D_L is the longitudinal dispersion coefficient, and s is the coordinate along the river centerline. Both D_L and K_2 are critical to the solution of this problem, and both have a significant uncertainty in prediction. For this application, equation (E9.2.1) has the following boundary conditions:

1. At $x = 0$ and $t = 0$, a total mass of $M = 100$ kg CCl_4 is released as a pulse into the river.
2. At $t \Rightarrow$ large, and $x \Rightarrow$ large, $C \Rightarrow 0$.

From analogy with Example 2.8, adding in a convection term, equation (E9.2.1)with these boundary conditions has solution

$$C = \frac{M/A_{cs}}{\sqrt{4\pi D_L t}} \exp\left[-\frac{(s-Ut)^2}{4D_L t} - K_2 t\right] \tag{E9.2.2}$$

The peak of equation (E9.2.2)occurs at $s = Ut$, so the peak concentration is given by

$$C_{\text{peak}} = \frac{M/A_{cs}}{\sqrt{4\pi D_L t}} e^{-K_2 t} \tag{E9.2.3}$$

The reaeration coefficient will indicate the transfer of CCl_4, because it is a volatile compound, as long as we use the correct Schmidt number in equation (9.7). At 20°C, CCl_4 has a diffusion coefficient of 1.2×10^{-9} m^2/s. Then, $Sc = 833$, and equation (9.7) gives $K_2 = 2.2 \times 10^{-5}$ s^{-1}.

As described in equation (6.59), longitudinal dispersion coefficient has a 67% confidence interval that is a factor of 1.7 times the best estimate. If the distribution of multiplicative uncertainty is normal, the 95% confidence interval would be at a factor of 3.4 times the best estimate. The reaeration coefficient has are MME of 1.8 for the Thackston and Krenkel equation (equation (9.7)). Again, if the multiplicative distribution is normal, the MME is 0.4 times the 95% confidence interval. Then the 95% confidence interval is a multiplicative factor of 4.5.

We will use the means and 95% confidence intervals for both D_L and K_2 to determine the time, and distance through $s = Ut$, when $C_{\text{peak}} = 0.0005$ g/m^3. These conditions are listed in Table E9.2.1, with the times determined through iteration on equation (E9.2.3). Table E9.2.1 shows that the peak value of concentration is no longer sensitive to longitudinal dispersion coefficient after roughly 3 days, because the peak is widely spread. The time when the water treatment plants downstream of the spill could turn on the water intake, however, would likely be sensitive to longitudinal dispersion coefficient.

The time and distance before the peak concentration of CCl_4 is below 0.5 ppb is sensitive to uncertainty in the value of K_2. We can see that, within a 95% confidence interval, the time when water intakes need to be turned off could vary between 0.8 and 12.4 days, or over 67 to 1,071 km of the Maipo River. The Maipo River, however, is not 1,071 km long, so the entire river below Puente Alto would need to be alerted.

Table E9.2.1: *Expected variation in the times and distance that water supply needs to be shut down on the Maipo River below the Puente Alto spill to maintain CCl_4 concentrations below 5 ppb*

D_L (m^2/s)	K_2 (/s)	t (s)	s (km)	t (hrs)	t (days)	Comments
20	2.2×10^{-5}	269,074	269	75	3.1	Best estimate
68	2.2×10^{-5}	243,829	244	68	2.8	$D_L \times 3.4$, upper CI
5.9	2.2×10^{-5}	294,435	294	82	3.4	$D_L/3.4$, lower CI
20	1.0×10^{-4}	66,703	67	19	0.8	$K_2 \times 4.5$, upper CI
20	5.0×10^{-6}	1,071,219	1,071	298	12.4	$K_2/4.5$, lower CI

CI, confidence interval.

B. Gas Transfer in Lakes, Estuaries, and Oceans

The influence of wind is predominant in determining the liquid film coefficient for lakes, reservoirs, oceans, and many estuaries. Wind creates a shear on the water surface and generates turbulence below and on the water surface. Thus, this section deals with the measurement and prediction of the wind influence on liquid film coefficient.

1. Opportunistic Measurement of Wind Influence

The opportunistic measurement techniques generally used are ^{14}C absorption and ^{222}Rn disequilibrium (Asher and Wanninkhof, 1998). First, there is an estimate of a long-term (~1,000 years) global gas transfer coefficient of $K_L = 6 \times 10^{-5}$ m/s, developed by assuming steady state between pre-1950 ^{14}C radioactive decay in the oceans and absorption from the atmosphere (Broecker and Peng, 1982). In addition, nuclear testing since 1950 has increased ^{14}C concentration in the atmosphere. Thanks to the atomic testing "battle" between the United States of America and the Soviet Union, we currently have a tracer that can be used on an oceanwide basis. A box model of an ocean basin is still needed. By using an appropriate oceanic model to estimate the depth of the interactive layer, and taking sufficient measurements of $^{14}CO_2$ at the ocean boundaries and inside the control volume, the fluxes and mean control concentration, respectively, can be determined. Then, the remainder of the flux is assigned to atmospheric fluxes of $^{14}CO_2$, and a liquid film coefficient is determined from a mass conservation equation:

$$V\frac{\partial {}^{14}C_{\text{basin}}}{\partial t} = \text{Ocean flux rate } ({}^{14}C_{\text{in}} - {}^{14}C_{\text{out}}) + K_L A({}^{14}C_{\text{atm}} - {}^{14}C_{\text{basin}}) \qquad (9.10)$$

where V is the volume of the interactive layer and A is the surface area of the ocean basin. An important consideration for these estimates is the depth of the interactive layer (Duffy and Caldera, 1995). The response time of equation (9.10) is on the order of years to decades, so any relationship to wind velocity is a long-term average.

By contrast, the gas transfer estimates utilizing ^{222}Rn measurements assumes steady state between ^{222}Rn production from radioactive decay of nonvolatile ^{226}Rd and gas transfer with the atmosphere. This assumption is possible because ^{222}Rn has a half-life of only 3.8 days, so accumulation and lateral ocean fluxes of ^{222}Rn is assumed to be minimal. Again, a potential problem is the active, versus inactive layer of the ocean; in this case, the mixed layer depth that may change during an experiment.

The results of both ^{14}C and ^{222}Rn measurements of liquid film coefficient versus wind velocity are plotted in Figure 9.4, along with two parameterizations that will be discussed in prediction of wind influence.

2. Measurement of Wind Influence with Deliberate Tracers

Batch Technique. As with river reaeration measurements, tracers can also be put into lakes, estuaries, and oceans to measure the influence of wind on liquid film coefficient. If we have a volatile tracer in a lake with a well-established mixed layer, for example, we can apply the same batch reactor equation from Section 6.A, as though we had a well-mixed tank:

$$V\frac{\partial C}{\partial t} = -K_L A\left(\frac{C_g}{H} - C\right) \tag{9.11}$$

where V is the volume of the mixed layer and A is the interfacial area. If we assume that C_g is a constant value, then we can assign $C' = Cg/H - C$, separate variables, and integrate to achieve

$$\ln\left(\frac{C - C_g/H}{C_0 - C_g/H}\right) = -K_L\frac{A}{V}(t - t_0) = -K_L a(t - t_0) \tag{9.12}$$

where C_0 is the concentration at $t = t_0$ and "a" is the specific surface area, which has units of length^{-1}. A plot of the log term in equation (9.12) versus time will result in a straight line of slope $K_L a$. If there are more than 11 points, the standard error of the slope is approximately the precision (random) uncertainty to the 67% confidence interval. That means that 67% of the data, if Gaussian around the mean, will fall within the confidence interval. Bias (systematic) uncertainty, of course, needs to be analyzed separately. There are other means of determining $K_L a$ for a batch reactor, the best known being the American Society of Civil Engineers (1992) technique that uses a nonlinear regression to determine C_g/H and $K_L a$.

The batch reactor analysis is a natural one to use for laboratory tanks and wind–wave facilities. In addition, it has been used for lakes, which are either well-mixed vertically or where the surface mixed layer is at close to a constant thickness (Livingstone and Imboden, 1993; Torgersen et al., 1982; Upstill-Goddard et al., 1990; Wanninkhof et al., 1987). Typically, sulfur hexafluoride (SF_6) or ^{3}He are used as deliberate gas tracers input to the lakes because they are detectable at low concentrations. The results of selected measurements are plotted versus the wind speed Reynolds number in Figure 9.5. The primary difference between the two sets of measurements is the fetch length of the water body, where the Upstill-Goddard et al. measurements were taken on a smaller water body. In general, the uncertainty of one given measurement

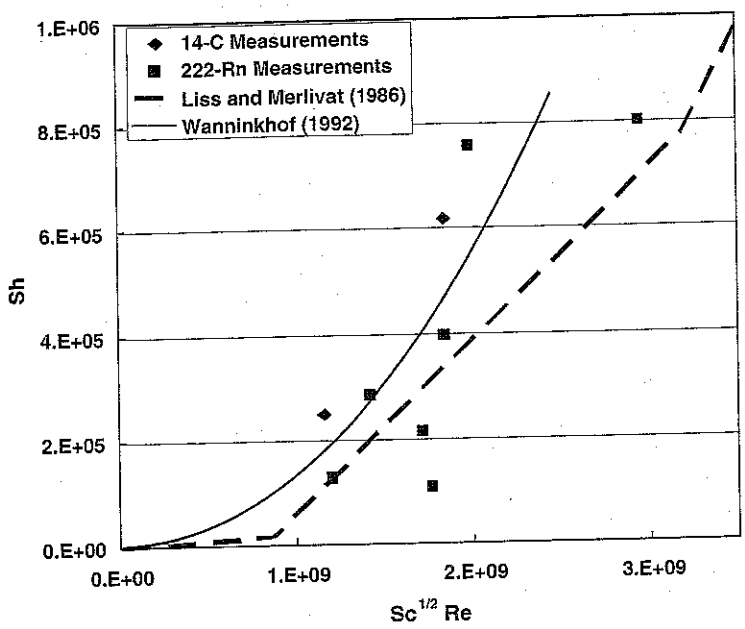

Figure 9.4. Sherwood number versus Reynolds number measured with ^{14}C and ^{222}Rn tracers. *Solid* and *dashed lines* are empirical relations developed from measurements.

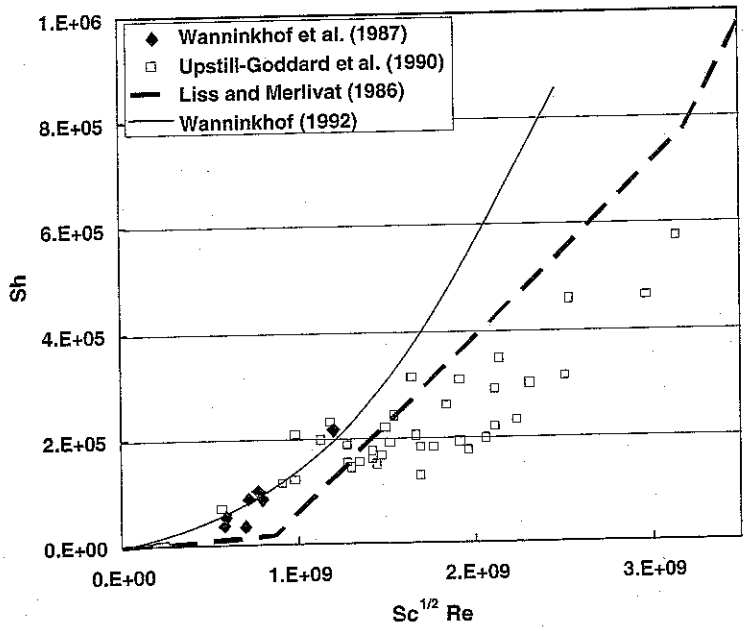

Figure 9.5. Sherwood number versus $Sc^{1/2}$ Re, measured by the batch reactor technique in small lakes. *Lines* represent equations developed from field measurements.

is large, but a number of measurements, taken together while leaving in the ones that give a negative K_L, results in the summary field measurements seen in Figure 9.5. The problem is that the investigator needs to be involved in deciding which measurements to average, so there is a potential bias in the results. Changes in mixed layer depth need to be taken into consideration, as well, if one is not able to assume a well-mixed lake.

Dual Tracer Technique. The dual tracer measurement technique utilizes two gas tracers with diffusion coefficients that are substantially different, such as ^{3}He and SF_6. This technique can also be utilized with one volatile (gas) tracer and one nonvolatile tracer. We will derive the relevant equations to determine liquid film coefficient from the diffusion equation for both cases, beginning with the two gas tracers.

Consider a cylindrical control volume of depth h that moves with the mean velocity of the tracer cloud containing two gas tracers, designated A and B. Using the cylinder as our control volume, the transport relation for each of the gas tracers can be written as

$$\frac{\partial \overline{C_i}}{\partial t} = D_x \frac{\partial^2 \overline{C_i}}{\partial x^2} + D_y \frac{\partial^2 \overline{C_i}}{\partial y^2} - \frac{K_L}{h} C_{si} \tag{9.13}$$

where $\overline{C_i}$ is the mean concentration of compound i over the column depth, D_y and D_x are the dispersion coefficients in the horizontal directions, and C_{si} is the concentration of compound i at the water surface. We will perform our mass balance on the ratio, $R = C_A/C_B$. Then, the derivative of R with respect to time is given as

$$\frac{\partial R}{\partial t} = \frac{\partial}{\partial t}\left(\frac{C_A}{C_B}\right) = \frac{1}{C_B}\left(\frac{\partial C_A}{\partial t} - R\frac{\partial C_B}{\partial t}\right) \tag{9.14}$$

Assuming that the dispersion of the ratio of concentrations to be small, we will ignore the dispersion of R, and equations (9.13) and (9.14) are combined to give

$$\frac{\partial R}{\partial t} = -\frac{1}{h}\left(K_{LA}R_{sA} - K_{LB}RR_{sB}\right) \tag{9.15}$$

where $R_{sA} = C_{sA}/\overline{C_B}$ and $R_{sB} = C_{sB}/\overline{C_B}$. We will assume the 1/2 power relationship between liquid film coefficient and diffusion coefficient and apply a surface renewal type of relationship. Then

$$\frac{K_{LB}}{K_{LA}} = \sqrt{\frac{D_B}{D_A}} \tag{9.16}$$

Substituting equation (9.16) into (9.15), and rearranging gives us an equation that can be used to develop K_{LA} from measurements of both tracers:

$$K_{LA} = -\frac{h}{\left(R_{sA} - \sqrt{\frac{D_B}{D_A}}RR_{sB}\right)}\frac{\partial R}{\partial t} \tag{9.17}$$

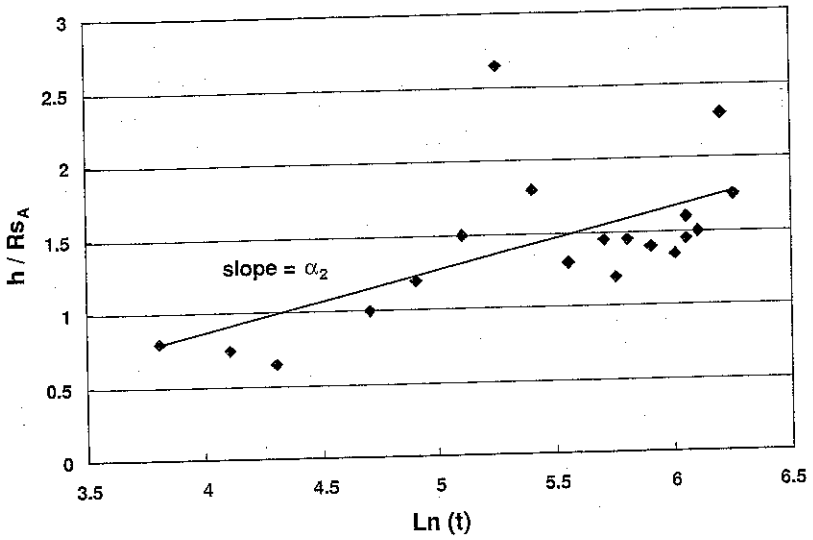

Figure 9.6. Measured data from a dual tracer cloud and the curve fit to the data.

R, R_{sA}, and R_{sB} can all be measured at various times. Then, a plot of the various terms in equation (9.17) will provide us with an estimate of K_L. If tracer B is nonvolatile, $K_{LB} = 0$, and equation (9.17) becomes

$$K_L = -\frac{h}{R_{sA}} \frac{\partial R}{\partial t} \tag{9.18}$$

Equation (9.17) applies to two volatile tracers and equation (9.18) to one volatile and one nonvolatile tracer.

Gulliver et al. (2002) applied equation (9.18) to field measurements of SF_6 and Rhodamine-WT, a nonvolatile tracer. Their analysis technique was as follows:

1. Regress $\ln(h/R_{sA})$ versus $\ln t$ in a linear regression. Then

$$h/R_{sA} = \alpha_1 t^{\alpha_2} \tag{9.19}$$

   where α_1 and α_2 are fitted constants. A sample for one data set, shown in Figure 9.6, indicates that there is considerable scatter, which is due to sampling uncertainty (i.e., one does not know if they are at the peak of the tracer cloud).
2. Regress R versus $t^{1-\alpha_2}$. The α_2 power is used to make the dimensions work out properly in the relation for K_L. Then

$$R = \alpha_3 t^{1-\alpha_2} + \alpha_4 \tag{9.20}$$

A sample of this regression is shown in Figure 9.7, again indicating considerable uncertainty. Equation (9.20) is chosen to result in the proper units for K_L. Combining equations (9.18) to (9.20) yields

$$K_L = \alpha_1 * t^{\alpha_2} * \left[\frac{\partial}{\partial t}\left(\alpha_3 * t^{(1-\alpha_2)} + \alpha_4\right)\right] \tag{9.21}$$

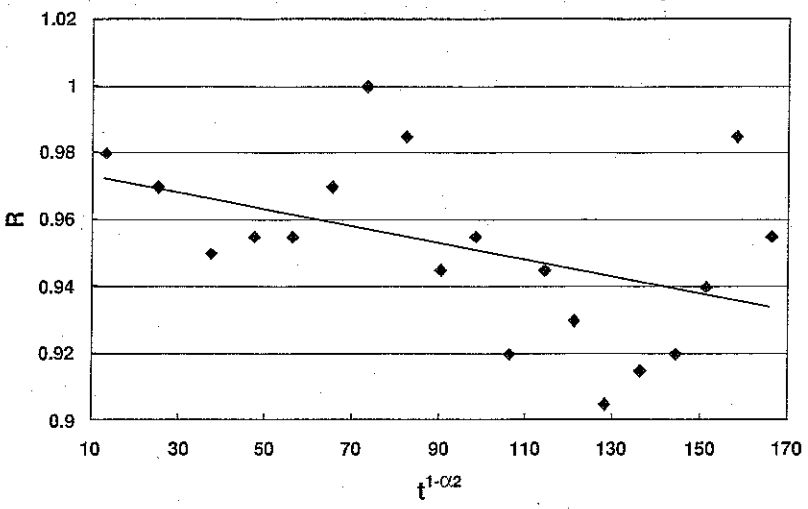

Figure 9.7. Measured data from a dual tracer experiment for 1 day and the curve fit to the data.

or

$$K_L = -\alpha_1 * \alpha_3 * (1 - \alpha_2) \tag{9.22}$$

With the dimensional formulation of equation (9.22), α_1 has units of length/time$^{\alpha 2}$ and α_3 has units of time$^{\alpha 2-1}$. Thus, K_L has units of length/time.

The precision uncertainty associated with field sampling is generally much larger than that associated with analytical technique, which is roughly $\pm 2\%$ to the 67% confidence interval for the two compounds used as conservative and gas tracers. A technique to determine the precision uncertainty associated with field sampling and incorporated into the mean K_L estimate will therefore be propagated with the first-order, second moment analysis (Abernathy et al., 1985):

$$U_{K_L}^2 = \left(U_{\alpha_1} * \frac{\partial K_L}{\partial \alpha_1}\right)^2 + \left(U_{\alpha_3} * \frac{\partial K_L}{\partial \alpha_3}\right)^2 + \left(U_{\alpha_2} * \frac{\partial K_L}{\partial \alpha_2}\right)^2 \tag{9.23}$$

When the partial derivatives are taken from equation (9.22), equation (9.23) becomes

$$U_{K_L}^2 = [\alpha_3 * (1 - \alpha_2) * U_{\alpha_1}]^2 + [\alpha_1 * (1 - \alpha_2) * U_{\alpha_3}]^2 + (\alpha_1 * \alpha_3 * U_{\alpha_2})^2 \tag{9.24}$$

The variables U_{α_1}, U_{α_2}, and U_{α_3} are the corresponding uncertainty values for each parameter. They are computed to the 67% confidence interval by taking the standard error of each parameter in the regressions (i.e., α_1, α_2 and α_3, and multiplying by their Student t-score t_S (i.e., $U_{\alpha_1} = t_S * SE_{\alpha_1}$), where t_S is the Student t-score at the confidence level of interest and $SE_{\alpha 1}$ is the corresponding standard error for the parameter α_1. The period can be chosen based on the maximum r^2 value or another statistical parameter. The results of four experiments are given in Figure 9.8.

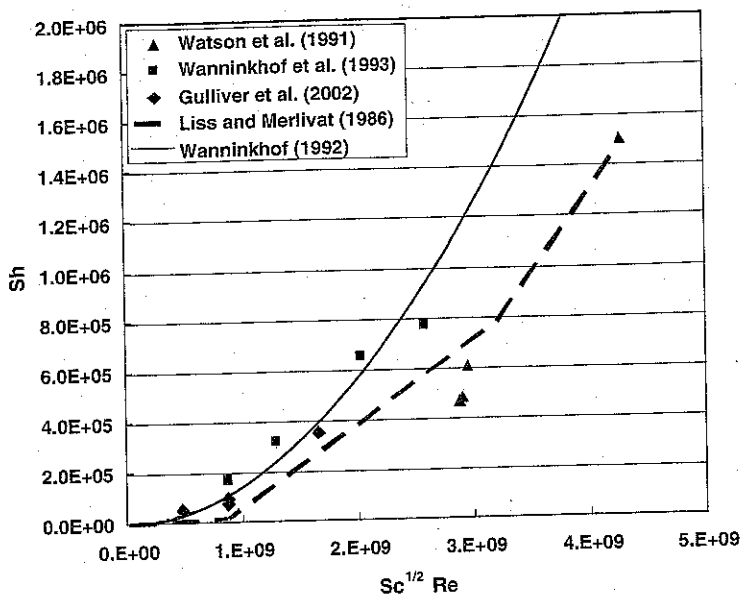

Figure 9.8. Sherwood number measured by the dual tracer technique versus Reynolds number.

Other investigators have used two measurements of the gas tracers taken over a longer time period (several days) and assumed that the cloud of tracers was well-mixed vertically. In this case, the following conditions must be met: (1) changes in the ratio of tracer concentrations caused by dispersion should be negligible compared with those resulting from gas transfer, (2) the water column should be well-mixed vertically, and (3) the experimental area should be close to constant depth. Criteria 1 is satisfied by having a tracer cloud that is large, compared with the depth and by staying close to the center of this cloud. Example 9.2 has shown us that, even at the peak of the concentration cloud, dispersion can have an impact on concentrations. With these assumptions, equation (9.17) becomes

$$\frac{1}{R}\frac{dR}{dt} = \frac{K_{LA}}{h}\left(1 - \sqrt{\frac{D_B}{D_A}}\right) \tag{9.25}$$

which can be integrated to give

$$K_{LA} = \frac{h}{\Delta t}\left(1 - \sqrt{\frac{D_B}{D_A}}\right)(\ln R_{t_2} - \ln R_{t_1}) \tag{9.26}$$

The results of these measurements are also given in Figure 9.8. Unfortunately, the technique utilizing equation (9.26) cannot provide an estimate of sampling uncertainty.

The data contained in Figures 9.4, 9.5, and 9.8 indicate similarity against wind velocity, even though the fetch length and size of the water bodies are different.

This is generally seen as an indication that wind is an important driving factor for lakes, estuaries, and oceans. It has been shown that breaking waves and water surface slicks are important (Asher and Wanninkhof, 1998), and there are other parameters – such as mean square water surface slope – that have been proposed as better indicators (Jähne, 1991). The problem is that our ability to predict these indicators from wind velocity measurements have not been developed and tested for liquid film coefficient.

One other measurement technique that has been used to measure K_L over a shorter time period, and is thus more responsive to changes in wind velocity, is the controlled flux technique (Hauβecker et al., 1995). This technique uses radiated energy that is turned into heat within a few microns under the water surface as a proxy tracer. The rate at which this heat diffuses into the water column is related to the liquid film coefficient for heat, and, through the Prandtl–Schmidt number analogy, for mass as well. One problem is that a theory for heat/mass transfer is required, and Danckwert's surface renewal theory may not apply to the low Prandtl numbers of heat transfer (Atmane et al., 2004). The controlled flux technique is close to being viable for short-period field measurements of the liquid film coefficient.

3. Prediction of the Wind-Influenced Gas Transfer Coefficient

There are two predictive relationships based on wind speed. Liss and Merlivat (1986) used a physical rationale to explain the increase in the K_L versus wind speed slope at higher wind velocities in wind–wave tunnel and lake measurements, resulting in a piecewise linear relationship with two breaks in slope. These breaks are presumed to occur at the transition between a smooth surface and a rough surface and between a rough surface and breaking waves. In dimensionless form, this relationship is given as

$$Sh = 3.4 \times 10^{-5} Sc^{1/3} Re \qquad U_{10} \geq 3.6\,\text{m/s} \tag{9.27a}$$

$$Sh = 1.9 \times 10^{-4} Sc^{1/2} (Re - Re_0) \qquad 3.6\,\text{m/s} < U_{10} \leq 13\,\text{m/s} \tag{9.27b}$$

$$Sh = 4.1 \times 10^{-4} Sc^{1/2} (Re - Re_b) \qquad 13\,\text{m/s} \leq U_{10} \tag{9.27c}$$

where U_{10} is the wind speed at 10 m above the mean water surface, $Sh = K_L L/D$, $Re = U_{10} L/\nu$, $Re_0 = 3.4\,\text{m/s}\, L/\nu$, and $Re_b = 8.3\,\text{m/s}\, L/\nu$. The length scale, L, could be any relevant length scale because it will drop out of the relationship when determining K_L.

Wanninkhof (1992) developed one relation from ^{14}C data:

$$Sh = 3.4 \times 10^{-5} Sc^{1/2} Re\, U_{10}\,(\text{m/s}) \tag{9.28}$$

Equation (9.28) does not lend itself to an easy conversion to dimensionless parameters because $K_L \sim U_{10}^2$. It is one equation, however, instead of three, which makes it

easier to use in computer programs and spreadsheets. If we assume that we are using $L = 10\,\text{m}$ and $\nu = 1 \times 10^{-6}\ \text{m}^2/\text{s}$, then equation (9.28) becomes

$$Sh = 3.4 \times 10^{-12} Sc^{1/2} Re^2 \tag{9.29}$$

Both equations (9.27) and (9.29) are compared with the existing field data in Figures 9.4, 9.5, and 9.8. With the scatter in the data, it is difficult to select one equation over another.

Jähne et al. (1984, 1987) proposed that liquid film coefficient is better related to mean water surface slope. Frew (1997) has found that the K_L relationship using mean square slope can be used to describe gas transfer with and without surface slicks. The problem with mean surface slope is that it cannot be accurately predicted for water bodies, because most investigators have emphasized the larger and longer waves, and the slope is most significant for the small, short waves. This will likely be the subject of future investigations.

C. Transfer of Nonvolatile Compounds

The evaporation of water is generally used to determine the gas film coefficient. A loss of heat in the water body can also be related to the gas film coefficient because the process of evaporation requires a significant amount of heat, and heat transfer across the water surface is analogous to evaporation if other sources and sinks of heat are taken into account. Although the techniques of Section 8.D can be used to determine the gas film coefficient over water bodies, they are still iterative, location specific, and dependent on fetch or wind duration. For that reason, investigators have developed empirical relationships to characterize gas film coefficient from field measurements of evaporation or temperature. Then, the air–water transfer of a nonvolatile compound is given as

$$J_A = K_G [C_A(z) - C_A(z = 0)] \tag{9.30}$$

where $C_A(z)$ is the concentration of compound A at an elevation z, which is typically the elevation of wind and temperature/humidity measurements to compute K_G.

The relationships developed from field measurements have been made dimensionless with the assumptions that $\nu = 1.33 \times 10^{-5}\ \text{m}^2/\text{s}$ and $D_{H_2O} = 2.6 \times 10^{-5}\ \text{m}^2/\text{s}$ to facilitate comparisons between relations and avoid dimensional problems. They are given in Table 9.2. The early measurements were to investigate the loss of water from the reservoirs of the Colorado River in the United States, and the later measurements were designed to investigate heat loss from heated water bodies. A revelation occurred in 1969, when Shulyakovskyi brought in buoyancy forces as related to natural convection to explain the heat loss from heated water at low wind velocities. This was picked up by Ryan and Harleman (1973), who realized that natural convection could explain the need for a constant term in front of the relationship for gas film coefficient, as had been found by Brady et al. (1969), Kohler (1954), Rymsha and Dochenko (1958), and Shulyakovskyi (1969). Finally, Adams et al. (1990) rectified

the overprediction of Ryan and Harleman's formulation at high wind velocities with the root sum of squares relation and brought in Harbeck's (1962) relation to include a term that represents fetch dependence.

By using the latent heat of vaporization for water, L_e, from equation (8.86), the previous relations for mass transfer can also be used for heat transfer due to evaporation:

$$\varphi_e = \frac{L_e K_G}{\rho C_P}(T_2 - T_s) \tag{9.31}$$

where ρ is the density of air and C_P is the heat capacity of air at constant pressure. We will compare the gas film coefficients from Table 9.2 in Example 9.3.

EXAMPLE 9.3: *Application of characteristic relations for gas film coefficient*

The WECAN, Inc. consulting company has a project that requires determining the evaporation from the 10 hectare cooling pond at the Hang Dog Power Facility, and they realized that they do not know how to determine the gas film coefficient. A table similar to Table 9.2 was found, and they decided to compare the resulting predictions to see if it made a significant difference. We will duplicate their results for one such comparison under the following conditions:

Water temperature, T_s, = 30°C
Air temperature, T = 10°C
Relative humidity at 2 m height = 40%
Air pressure = 1 atm
Various wind velocities up to 15 m/s

The *Handbook of Chemistry and Physics*, or some of the material in the Appendix A–3, can be used to determine the following fluid properties:

$\nu = 1.33 \times 10^{-5}$ m^2/s
$D = 2.4 \times 10^{-5}$ for water vapor, from Chapter 3
$\alpha = 2.0 \times 10^{-5}$ m/s

Now, virtual temperature is given by the equation

$$\Delta\theta_v = \| T_s(1 + 0.378 p_{vs}/P_a) - T_a(1 + 0.378 p_{va}/P_a), 0 \| \tag{8.73}$$

and saturation vapor pressure will be required to compute virtual temperature:

$$p_{vs}(mb) = 6.11 \exp\left\{\frac{17.3[T(°\text{K}) - 273]}{T(°\text{K}) - 35.9}\right\} \tag{8.74}$$

Then, p_{vs}/P_a = 0.042 at 30°C and = 0.012 at 10°C, and

$$p_{va} = \frac{RH}{100} p_{vs} \tag{8.75}$$

Table 9.2: *Relationships developed to characterize gas film coefficient over water surfaces*

Investigator	Formula	Water body
Adams et al. (1990)	$Sh = \left[\left(0.125\,Ra_V^{1/3}\right)^2 + \left(0.0061\,Sc\,Re^{0.933}\,\hat{W}^{0.033}\right)^2\right]^{1/2}$	East Mesa Geothermal Facility and cooling ponds
Brady et al. (1969)	$Sh = 0.049\left(\frac{Ra}{\beta_T \Delta T}\right)^{1/3} + 9.6 \times 10^{-6}\,Sc\,Re^{1/3}\,\hat{W}^{1/3}$	Power plant cooling ponds
Ficke (1972)	$Sh = 0.0019\,Pe$	Pretty Lakes, Ind
Gulliver and Stefan (1986)	$Sh = 0.125\,Ra_V^{1/3} + 0.0013\,Pe$	Heated streams
Harbeck (1962)	$Sh = 0.0061\,Sc\,Re^{0.933}\,\hat{W}^{0.033}$	Various reservoirs
Harbeck et al. (1958)	$Sh = 0.002\,Pe$	Lake Mead, Ariz
Hughes (1967)	$Sh = 0.0014\,Pe$	Salton Sea, Calif
Kohler (1954)	$Sh = 0.011\left(\frac{Ra}{\beta_T \Delta T}\right)^{1/3} + 7.5 \times 10^{-5}\,Pe$	Lake Hefner, Ariz
Marciano and Harbeck (1954)	$Sh = 0.0017\,Pe$	Lake Hefner, Ariz
Ryan and Harleman (1973)	$Sh = 0.125\,Ra_V^{1/3} + 0.0016\,Pe$	Cooling ponds
Rymsha and Dochenko (1958)	$Sh = 0.042\left(\frac{Ra}{\beta_T \Delta T}\right)^{1/3} + 0.0125\,Ra^{1/3} + 0.0016\,Pe$	Various rivers, heated in winter
Turner (1966)	$Sh = 0.0031\,Pe$	Lake Michie, NC
Shulyakovskyi (1969)	$Sh = 0.031\left(\frac{Ra}{\beta_T \Delta T}\right)^{1/3} + 0.125\,Ra_V^{1/3} + 0.0017\,Pe$	Various water bodies
	$Sh = \frac{K_G A^{1/2}}{D} \quad Ra = \frac{g\beta_T \Delta T A^{3/2}}{D\nu}$	
	$Pe = \frac{W A^{1/2}}{\nu} \quad Ra_V = \frac{g\beta_T \Delta T_V A^{3/2}}{D\nu} \hat{W} = \frac{W^2}{g A^{1/2}}$	

K_G, gas film coefficient; A, surface area of water body; D, diffusion coefficient of compound in air; W, wind velocity at 2 m above the mean water surface; ν, kinematic viscosity of air; α, thermal diffusion coefficient of air; g, acceleration of gravity; β_T, thermal expansion coefficient of moist air; ΔT, temperature difference between water surface and 2 m height; ΔT_V; virtual temperature difference between water surface and 2 m height.

So that $p_{va}/P_a = 0.005$. Then, $\Delta\theta_V = 20.5°C$. Finally,

$$\beta_T = \frac{1}{T_{av}(°C) + 273} \tag{8.76}$$

So that $\beta_T = 3.29 \times 10^{-3} °K^{-1}$. The results for five formulas are given in Figure E9.3.1. The major differences are the slope at high wind speeds and the intercept at a wind velocity of 0. Probably the best documented is the relation of Adams et al. (1990), which used much of the previous field data and tested the results on two additional water bodies at a variety of buoyancy parameters. This relation transitions between the Ryan and Harleman (1973) equation at low wind velocity and that of Harbeck (1962) at a higher wind velocity.

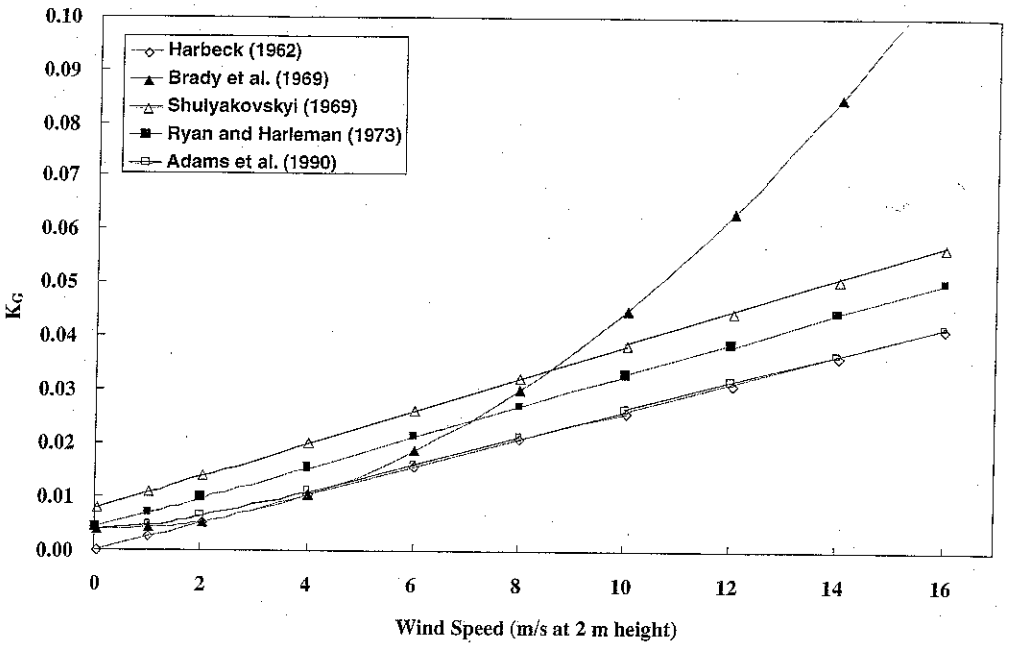

Figure E9.3.1. Comparison of five formulas for gas transfer coefficient versus wind speed for example 9.3.

D. Gas Transfer from Bubbles

Measurement of Liquid Film Coefficient

To determine the liquid film coefficient for gas transfer from or into bubbles, dissolved oxygen and dissolved nitrogen concentrations must be measured (Schierholz et al. 2006) This is possible with a polargraphic probe for dissolved oxygen and a total gas meter, which measures the pressure of gas in equilibrium with the water. Nitrogen (+ argon) concentration is found by subtraction of dissolved oxygen and water vapor from total gas concentration. Then, the equations in Section 8.F may be used to determine the value of $K_L A_b$ and K_{LS} that will give these concentration measurements. Equation (8.102) changes with depth as z and y_m change with depth. The boundary condition of equations (8.101) and (8.102) is the gas molar ratio at the sparger, which is 0.266 for air and the initial concentrations C_O and C_N in the liquid. The equations are then solved from $z = h_d$ to $z = 0$ at one moment in time and used to compute C_O and C_N in equation (8.90) for the next time step. The resulting concentration curves are adjusted by changing $K_{LO}A_b$ and K_{LSO} until the concentration versus time curves match the measured one for C_O. Thus, two transfer coefficients, $K_{LO}A_b$ and K_{LSO}, can be determined.

Schierholz et al. (2006) applied equations (8.98) to (8.102) to various tank experiments of depths that varied from 2.25 to 32 m in depth. The results were that a value of the bubble transfer coefficient, $K_L A_b/V$and the surface transfer coefficient, K_{LS},

could be determined. The following relationship were fit to the resulting bubble–water transfer coefficients:

$$Sh = \frac{1}{6}\frac{We^{3/5}Sc^{1/2}\ Re}{Fr} \qquad \text{Fine bubble diffusers} \tag{9.32}$$

and

$$Sh = \frac{1}{37}\frac{We^{3/5}Sc^{1/2}\ Re}{Fr} \qquad \text{Course bubble diffusers} \tag{9.33}$$

where $Sh = K_L A_b h_d^2/DV$, $We = U^2 h_d \rho/\sigma$, $Sc = \nu/D$, $Re = Uh_d/\nu$, and $Fr = U/\sqrt{gh_d}$ is the Froude number. In the dimensionless numbers, h_d is diffuser depth, V is the volume of the water body, and U is the superficial gas velocity, Q_a/A_{cs}, where Q_a is the air discharge at standard temperature and pressure and A_{cs} is the cross-sectional area of the water body or tank. A fine bubble diffuser has a bubble diameter leaving the diffuser that is less than roughly 4 mm in diameter. The resulting water surface transfer coefficients were fit to the following equation:

$$Sh_s = 49\, Sc^{1/2}\ Re \left(\frac{A_{cs}}{h_d^2}\right)^{0.72} \tag{9.34}$$

where Sh_s is the Sherwood number for surface transfer, $K_L A_s/(h_d D)$, and A_s is the surface area of the water body. It is interesting that K_{Ls} is linearly dependent on gas flow rate. This is likely because the bubbles passing through the surface create a significant free-surface turbulence. Of course, these tests were performed without wind or a mean flow, so any wind or low influence would need to be somehow factored in. Figures 9.9 and 9.10 provide the data analysis results and the curvefits of the characteristic equations.

EXAMPLE 9.4: *Sizing bubble diffusers for a reservoir with combined sewer overflow*

The McCook, Thornton, and O'Hare reservoirs make up the Chicago-land Underflow Plan, an integral part of Chicago's $3 billion Tunnel and Reservoir Plan. This system of intercepting sewers, dropshafts, tunnels, and reservoirs will capture and store combined sewage and stormwater until municipal water reclamation plants can treat it. Applying equations (9.31) through (9.33), and equations (8.90), (8.101), and (8.102), both a coarse bubble and a fine bubble aeration system for the McCook reservoir in Chicago can be designed. The aeration design needs to maintain aerobic conditions in the reservoir (at least 2 mg/L) that has a designed area of 395,300 m^2. The 1-in-100-year event in July should cause the McCook Reservoir to fill to its maximum level of 73 m (Robertson, 2000). When the reservoir is at its maximum elevation after a big flood, the biochemical oxygen demand (BOD) will be lower because of dilution of the sanitary sewage with stormwater. A 5-day BOD design range of 30 mg/L when full to 80 mg/L when at the lowest depth of 10 m is estimated and a BOD decay rate of 0.25 d^{-1} is assumed. Other design criteria are that the diffusers will be 1 m above the bottom of the reservoir, the maximum air flow rate per

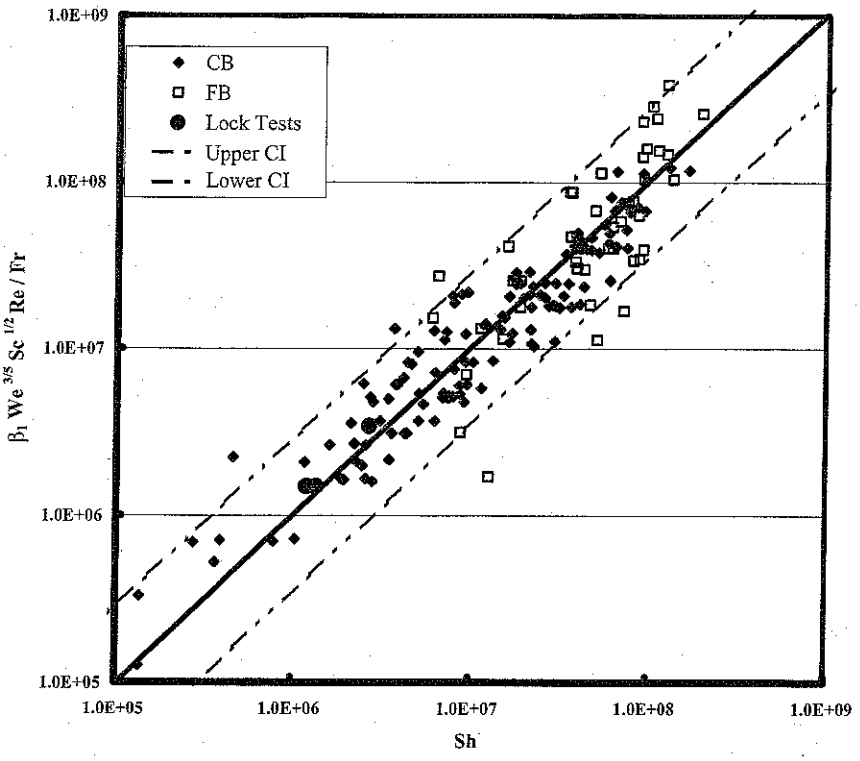

Figure 9.9. Characterization of the bubble mass transfer coefficients for Tank tests. Coarse bubble (CB) $\beta_1 = 1/36$, and fine bubble (FB) $\beta_1 = 1/6$. The 95% confidence interval is included (CI) (Schierholz et al. 2006).

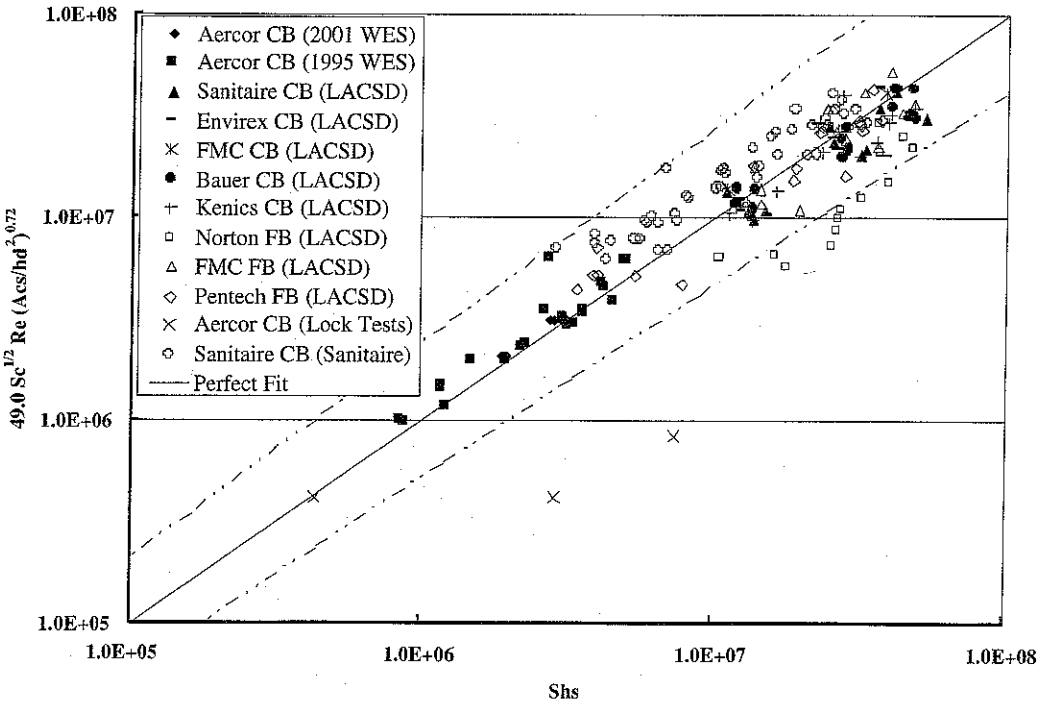

Figure 9.10. Characterization of the surface mass transfer coefficients for the tank tests. The 95% confidence interval is included (Shierholz et al., 2006). CB, coarse bubble; FB, fine bubble; LACSD, Los Angeles County Sanitary District; WES, U.S. Army Engineer Waterways Experiment Station.

coarse bubble diffuser is 100 scmh, and the maximum air flow rate per fine bubble diffuser is 20 scmh.

Using an iterative procedure between equations (8.88) through (8.102) and equations (9.32) through (9.34), an aeration system to accommodate the BOD range can be designed. Using coarse bubble diffusers and the high BOD of 80 mg/L, assumed to occur at a depth of 10 m, it was determined that a single coarse bubble diffuser with an air flow rate of 100 scmh would maintain aerobic conditions for an area of 341 m^2 with the above conditions. Based on this, 1,160 coarse bubble diffusers supplying a total air flow of 116,000 scmh would be needed for the McCook Reservoir. For this case, $K_L A_b = 0.063\,hr^{-1}$ and $K_L A_s = 0.064\,hr^{-1}$.

The air flow of the coarse bubble aeration system was then adjusted for the lower BOD of 30 mg/L that is assumed to occur at a depth of 73 m, with each of the 1,160 diffusers maintaining 2 mg/L in a 341 m^2 area. An air flow rate of 29 scmh per diffuser (33,640 scmh total) was determined to be sufficient, assuming that the characteristic equations may be extrapolated to 73 m of depth. For this case, $K_L A_b = 0.018\,hr^{-1}$ and $K_L A_s = 0.003\,hr^{-1}$. During the high BOD period at 10 m depth, approximately 3.5 times as much air flow is needed to maintain aerobic conditions.

A fine bubble aeration system for McCook Reservoir was designed using the same procedure. The system was first designed for the high BOD of 80 mg/L and a depth of 10 m. It was determined that a fine bubble diffuser with an air flow rate of 20 scmh would maintain aerobic conditions for an area of 115 m^2. From this, 3,438 fine bubble diffusers supplying a total air flow of 68,760 scmh would be needed for the reservoir. For this case, $K_L A_s = 0.003\,hr^{-1}$ and $K_L A_s = 0.044\,hr^{-1}$.

The air flow of the fine bubble system was then adjusted for the lower BOD of 30 mg/L and 73 m depth. With each of the 3,438 diffusers maintaining 2 mg/L in a 115 m^2 area, an air flow rate of 3.8 scmh per diffuser (13,065 scmh total) was determined. For this case, $K_L A_b = 0.034\,hr^{-1}$ and $K_L A_s = 0.001\,hr^{-1}$. During the high BOD period, approximately 5.3 times as much air flow is needed to maintain aerobic conditions.

A coarse bubble aeration system for McCook Reservoir requires only 1,160 diffusers, approximately one-third of the 3,438 diffusers needed for a fine bubble aeration system. However, significantly less air flow is needed for the fine bubble diffusers in comparison with the coarse bubble diffusers. At the more common depth of 10 m, the air flow required by the fine bubble diffusers was 39% of that required by the coarse bubble diffusers. These considerations and the mixing requirements of the reservoir are a part of the aeration system design.

Although the process to determine $K_L A_s$ and K_{Ls} is possible with a spread sheet, it is cumbersome for commercial specifications. The guideline for the testing of commercial aeration devices has been well developed and is generally available (American Society of Civil Engineers, 1992). There is no requirement to measure total dissolved gas pressure or estimate dissolved nitrogen concentration, and an

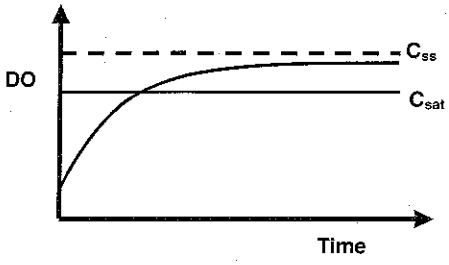

Figure 9.11. Disturbed equilibrium for the determination of the coefficients $K_L a$ and C_{ss}. DO is dissolved oxygen concentration, and C_{sat} is the saturation concentration at equilibrium with the atmosphere, which is generally below C_{ss}.

equation similar to equation (9.11) is fit to concentration versus time data for diffuser measurements in clean water:

$$\frac{\partial C}{\partial t} = -K_L a\,(C_{ss} - C) \tag{9.35}$$

with solution

$$\ln\left[\frac{C_{ss} - C}{C_{ss} - C(t=0)}\right] = -K_L a t \tag{9.36}$$

where C is the dissolved oxygen concentration, $K_L a$ is a coefficient that represents liquid film coefficient times surface area divided by the volume of the water body, and C_{ss} is the steady-state concentration of dissolved oxygen that is determined from the fitting procedure. The tests are run such that dissolved oxygen concentration is reduced chemically, by adding sodium sulfite, or physically, such as through stripping with nitrogen gas, as illustrated in Figure 9.11. The dissolved oxygen concentration is recorded as it moves from the temporary reduction back to a steady-state concentration, C_{ss}. The values of $K_L a$ and C_{ss} are curve fit to these measurements. Either equation (9.35) or (9.36) can be fit to a concentration curve like the one given in Figure 9.11, varying C_{ss} and $K_L a$ until an optimum fit is achieved. The drawback to this technique is that $K_L a$ represents an unknown combination of $k_{LS}A_s/V$, $k_{Lb}A_b/V$, and depth, so the tests must be at the application depth.

Of course, both of the two coefficients, C_{ss} and $K_L a$ are some combination of the processes considered when equation (8.87) through (8.102) were developed, and are a function of liquid film coefficient across both the bubbles and the free surface, bubble and water surface interfacial area, hydrostatic pressure, the mole ratio of gas in the bubbles, and equilibrium with the atmosphere. These two coefficients, however, can be valuable in the design of an aeration system, as long as (1) the arrangement of diffusers in the water body or tank is similar to the application and (2) the depth of the test is the same as the application. Significant deviations from these two criteria will cause errors in the application of the tests to the field.

E. Problems

1. The effluent from a sewage treatment plant on a river with an upstream biochemical oxygen demand (BOD) of 2 g/m^3 has a discharge of 10 m^3/s and a BOD of 15 g/m^3. Determine the best choice of stream reaeration coefficient,